No study has yet compared the exon skipping due to identical antisense PMOs between cells of different species carrying same exon deletion in mRNA. Recent investigations have reported a limitation in designing efficient antisenses to induce human dystrophin skipping in a mice model assay [25]; however, we confirmed the feasibility of direct translation of an antisense PMO from a DMD dog model to a DMD patient, at least *in vitro*, for the first time.

The four-antisense PMO cocktail, the addition of a fourth antisense sequence to the three-antisense PMO cocktail, increased the efficiency of skipping as previously reported [26,27]. The effectiveness of the four-antisense PMO cocktails, however, must be evaluated *in vivo*, and we are planning systemic treatment of $CXMD_J$ with them. Our results underscore the usefulness of $CXMD_J$ as a DMD model for translational research and advance the prospect that systemic treatment of the DMD patient by multi-exon skipping is possible.

Mode of exon 9 skipping might be affected by frequency of alternative splicing

With the antisense PMO targeting exons 6 and 8, exon 9 was always skipped in $CXMD_J$, although it was only partially skipped in DMD 8772. Two possibilities were considered to explain the difference: (1) the effects of the shortened introns 6 and 7 due to the deletion around exon 7 in DMD 8772 (**Figure 5**), and (2) the different frequencies of alternative splicing of exon 9. For the former case, we tried exon 8 skipping using a combination of Ex8A and Ex8G in normal and affected human MyoD-transduced fibroblasts, and found that the skipping of exon 8 and exons 8/9 happened simultaneously (**Figure S1**). Therefore, it is unlikely that the intron length affects the difference. In the latter case, the untreated MyoD-transduced fibroblasts from $CXMD_J$ clearly showed one normal and one alternative transcript; on the other hand, the untreated sample from DMD 8772 showed only a normal transcript, suggesting that the frequency of alternative splicing of exon 9 is an underlying factor in the difference. It was reported that an antisense oligonucleotide targeting exon 8 facilitates the skipping of exon 9 as well as exon 8 by effecting the concatenation of exons 8 and 9 in human and dog cells [28].

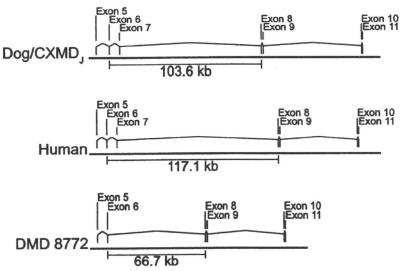

Figure 5. Location of dystrophin exons 5 to 11 in the genome. Distances from dystrophin exon 6 to exon 8 are indicated based on the GenBank reference sequences of *Canis familiaris* chromosome X genomic contig, whole genome shotgun sequence (NW_879562.1) and *Homo sapiens* 211000035840903 genomic scaffold, whole genome shotgun sequence (CH471074.1).
doi:10.1371/journal.pone.0012239.g005

These findings were observed in myoblasts but not in MyoD-tansduced fibroblasts [29,30,31]. As is well known, the mode of alternative splicing differs among various tissues [32,33], and our MyoD-transduced fibroblasts might have characteristics that are incompatible with the alternative splicing of exon 9.

In summary, MyoD transduction of fibroblasts with the help of FACS may be practical for exon skipping assays, and the direct translation of an antisense PMO from a DMD dog model to a DMD patient was feasible *in vitro*, suggesting that the animal model-based antisense PMO for multiple skipping could be effective for humans as well.

Materials and Methods

Ethics Statement

The patient samples were collected and used with the approval of the Ethics Committee of the National Center of Neurology and Psychiatry, approval ID: 20-4-6. Written informed consent was obtained from the donor. The dog study was approved by the Ethics Committee for the Treatment of Middle-sized Laboratory Animals of the National Center of Neurology and Psychiatry, approval ID: 20-05.

Cell culture

Dog primary myoblasts and fibroblasts were obtained from muscle specimens of normal and affected neonatal dogs of the $CXMD_J$ colony using a standard pre-plating technique. Primary fibroblasts of the DMD patient (DMD 8772) were obtained from skin explants and peripheral blood lymphocytes using Lymphocyte Separating Medium (PAN Biotech GmbH, Aidenbach, Germany). Lymphoblastoid cell lines were established by transformation with Epstein-Barr virus. The normal human fibroblast cell line TIG-119 was obtained from the Health Science Research Resource Bank (Osaka, Japan). Fibroblasts were cultured in 20% or 10% growth medium containing DMEM/F-12 1:1 (Invitrogen, San Diego, CA, USA), 20% or 10% fetal bovine serum, and 1% penicillin/streptomycin. For differentiation to myotubes, FACS-sorted MyoD-transduced fibroblasts were cultured in 2% differentiation medium containing DMEM/F-12 1:1, 2% horse serum, ITS Liquid Media Supplement (Sigma-Aldrich, St. Louis, MO, USA), and 1% penicillin/streptomycin.

Genomic mutation analysis

The dystrophin exon 7-deletion of DMD 8772 had been identified previously by MLPA. For breakpoint detection, lymphocyte genomic DNA was used as a template. Seven pairs of intron-spanning primers, positioned in the intron 6/7, were designed to yield 150-600 bp PCR products. A failure of PCR indicated deletions spanning the primer annealing sites. Four of seven primer pairs showed no amplification, suggesting that the deletion was more than 3.5 kb and less than 64.4 kb. Additionally, two intron 6 sense-primers and eight intron 7 antisense-primers were designed. Each primer pair was placed by flanking the breakpoint and expected to yield PCR products within the range of 4–64 kb. Primer sequences are available on request. PCR was performed using Phusion Hot Start High-Fidelity DNA Polymerase (Finnzymes, Keilaranta, Finland), and the cycling program was set to yield 16 kb products with a program of 35 cycles of 98°C for 10 sec, 60°C for 30 sec, and 72°C for 450 sec. Failure of PCR indicated products of more than 16 kb in size or the deletion of annealing sites. The breakpoint region was thus narrowed down to 2.5 kb, then primer walk sequencing was performed (Operon Biotechnologies, Tokyo, Japan).

MyoD transduction and cell sorting by FACS

The coding sequences of mouse *Myod1* (CCDS 21277.1) and human *MYOD1* (CCDS 7826.1) were derived from the Consensus CDS database [34]. The sequences were synthesized and cloned into a pUC57 vector (GenScript, Piscataway, NJ, USA). We subcloned it into a pRetroX-IRES-ZsGreen1 expression vector (Clontech, Mountain View, CA, USA). The expression vector, a pVSV-G envelope vector, and a gap-pol expression vector were co-transfected into a 293T packaging cell line using the standard calcium phosphate method. After 48–72 h incubation, the viral supernatant was collected and stored at −80°C. For retroviral transduction, the fibroblasts were harvested at 70–80% confluence in a T225 flask, and 2.5 ml thawed retroviral stock was added to 35 ml of growth medium. We added polybrene (Sigma-Aldrich) to a final concentration of 8 μg/ml. After 48–72 h incubation at 32°C, the culture medium was replaced with fresh growth medium, the cells were incubated at 37°C 1–3 d more, until the GFP-positive cells exceeded approximately 60%. Cell sorting was performed on a FACS VantageSE or FACSAria flow cytometry system (BD Bioscience, Franklin Lakes, NJ, USA). The recovered GFP-positive cells were seeded in Matrigel (BD Bioscience)-coated well plates at density of 5×10^4 cell/cm^2. After confirmation of cell attachment, the culture medium was changed to 2% differentiation medium. We cultured MyoD-transduced fibroblasts for 10 to 16 d to differentiate to myotubes.

Antisense PMO design and transfection to cultured cells

The antisense PMO sequences Ex6A, Ex6B, and Ex8A were described in Yokota et al. [6]. In addition, extra sequences hEx6B, Ex8G, Ex8I, and Ex8K were designed and synthesized (Gene Tools, LLC, Philomath, OR, USA). We used the Human Splicing Finder for *in silico* prediction of the splice-enhancer motifs [35]. All sequences are shown in **Table S1**. We transfected the antisense PMOs into myotubes differentiated from MyoD-transduced fibroblasts with a transfection agent, Endo-Porter (Gene Tools). In the 2% differentiation medium, the final concentration of the antisense PMO was 10 μM for a single sequence, 20 μM for two sequences, and a total of 30 μM for three or four sequences. A final concentration of Endo-Porter was 6 μM. After 48–72 h incubation with the PMO, the medium was changed to a fresh culture medium free of PMOs. The cells were recovered for analysis after 24–48 h in the PMO-deprived medium to allow sufficient time to translate dystrophin protein.

Quantitative RT-PCR analysis

Total RNA was extracted from MyoD-transduced fibroblasts obtained from normal subjects using Trizol (Invitrogen) at the time points specified. Total RNA (100-200 ng) was employed for cDNA synthesis using a QuantiTect Reverse Transcription Kit (Qiagen, Hilden, Germany). Quantitative real-time PCR was performed using ExTaq II SYBR (Takara, Kyoto, Japan) and a MyiQ Single-Color Real-Time PCR detection system (Bio-Rad, Hercules, CA). Primer sequences are shown in **Table S2**. Expression of dystrophin mRNA was normalized to *GAPDH* mRNA, and the time course of the increment was calculated by the delta-delta-Ct method.

RT-PCR and sequence analysis

As well as quantitative RT-PCR analysis, total RNA extraction and cDNA synthesis were performed. For myoblasts and MyoD-transduced fibroblasts, 35 cycles of denaturing at 98°C for 10 sec, annealing at 63°C for 30 sec, and extension at 72°C for 1 min were performed with ExTaq DNA polymerase (Takara). For fibroblasts and lymphoblasts, nested PCR was performed. Primer sequences are shown in **Table S3**. PCR products were electrophoresed on 1.2% SeaKem LE agarose gel (Lonza, Basel, Switzerland). The bands of interests were excised using a Wizard SV Gel and PCR Clean-Up system (Promega, Fitchburg, WI, USA), then sequenced directly or cloned into a vector using a TOPO-TA Cloning Kit (Invitrogen) with standard cloning techniques. Sequencing was performed by Fasmac Corporation (Kanagawa, Japan).

Immunostaining analysis

Cells were fixed in 3% paraformaldehyde, permeabilized in 10% Triton-X, then blocked by 10% goat serum in PBS for 1 h at room temperature. The cells were incubated with the primary antibody for 1 h at room temperature using anti-dystrophin (NCL-Dys1, diluted 1:30, Novocastra, Newcastle upon Tyne, UK), anti-myosin heavy chain (NCL-MHCf, diluted 1:30, Novocastra), anti-MyoD (NCL-MyoD1, diluted 1:30, Novocastra), or anti-desmin (NCL-DES-DERII, diluted 1:30, Novocastra). Incubation with the secondary antibody was performed for 30 min at room temperature using anti-rabbit or anti-mouse IgG (Alexa Fluor 546 highly cross-adsorbed, diluted 1:300, Invitrogen). Antibodies were diluted in Can Get Signal Immunostain A solution (Toyobo, Osaka, Japan). To visualize nuclei and enhance fluorescence signals, cells were mounted with Pro Long Gold Antifade reagent (Invitrogen).

Immunoblotting analysis

Protein was extracted from cultured cells using RIPA buffer (Thermo Fisher Scientific, Rockford, IL, USA) containing Complete Mini (Roche Applied Science, Indianapolis, IN, USA) as a protease inhibitor. Protein concentrations were determined using a BCA protein assay kit (Thermo Fisher Scientific) and equalized. After being mixed with an equal volume of EzApply sample buffer (ATTO Corporation, Tokyo, Japan), cell lysates containing equal amounts of total protein were denatured at 95°C for 5 min, electrophoresed in NuPAGE Novex Tris-Acetate Gel 3–8% (Invitrogen) at 150 V for 75 min, and transferred onto an Immobilon-P membrane (Millipore Corp., Billerica, MA, USA). Membranes were blocked for 1 h with 5% ECL Blocking agent (GE Healthcare, Buckinghamshire, UK) and probed with anti-dystrophin antibody (NCL-Dys1, diluted 1:50, Novocastra), followed by incubation with peroxidase-conjugated goat-anti-mouse IgG (Bio-Rad). An ECL Plus Western blotting system (GE Healthcare) was used to detect protein bands.

Supporting Information

Figure S1 RT-PCR of dystrophin mRNA isolated from the normal and affected human MyoD-transduced fibroblasts after the single exon 8 skipping.
Found at: doi:10.1371/journal.pone.0012239.s001 (0.30 MB PDF)

Table S1 Sequences of antisense PMO for dystrophin gene (for dog and human if not specified).
Found at: doi:10.1371/journal.pone.0012239.s002 (0.07 MB PDF)

Table S2 Sequences of qRT-PCR primers.
Found at: doi:10.1371/journal.pone.0012239.s003 (0.07 MB PDF)

Table S3 Sequences of RT-PCR primers.
Found at: doi:10.1371/journal.pone.0012239.s004 (0.07 MB PDF)

Acknowledgments

The authors thank Yu-ichi Goto (Department of Mental Retardation and Birth Defect Research, National Center of Neurology and Psychiatry), Narihiro Minami (Department of Neuromuscular Research, National Center of Neurology and Psychiatry), Hirofumi Komaki (Department of Child Neurology, National Center of Neurology and Psychiatry), Katsutoshi Yuasa (Research Institute of Pharmaceutical Sciences, Faculty of Pharmacy, Musashino University, Tokyo, Japan), and Tetsuya Nagata, Yuko Shimizu, and Satoru Masuda (Department of Molecular Therapy, National Center of Neurology and Psychiatry) for useful discussions and technical assistance.

Author Contributions

Conceived and designed the experiments: TS AN ST. Performed the experiments: TS YA. Analyzed the data: TS MO. Contributed reagents/materials/analysis tools: TY TO. Wrote the paper: TS AN ST.

References

1. Aartsma-Rus A, Bremmer-Bout M, Janson AA, den Dunnen JT, van Ommen GJ, et al. (2002) Targeted exon skipping as a potential gene correction therapy for Duchenne muscular dystrophy. Neuromuscul Disord 12(Suppl 1): S71–77.
2. Mann C, Honeyman K, Cheng A, Ly T, Lloyd F, et al. (2001) Antisense-induced exon skipping and synthesis of dystrophin in the mdx mouse. Proc Natl Acad Sci U S A 98: 42–47.
3. Alter J, Lou F, Rabinowitz A, Yin H, Rosenfeld J, et al. (2006) Systemic delivery of morpholino oligonucleotide restores dystrophin expression bodywide and improves dystrophic pathology. Nat Med 12: 175–177.
4. van Deutekom J, Janson A, Ginjaar I, Frankhuizen W, Aartsma-Rus A, et al. (2007) Local dystrophin restoration with antisense oligonucleotide PRO051. N Engl J Med 357: 2677–2686.
5. Kinali M, Arechavala-Gomeza V, Feng L, Cirak S, Hunt D, et al. (2009) Local restoration of dystrophin expression with the morpholino oligomer AVI-4658 in Duchenne muscular dystrophy: a single-blind, placebo-controlled, dose-escalation, proof-of-concept study. Lancet Neurol 8: 918–928.
6. Yokota T, Lu Q, Partridge T, Kobayashi M, Nakamura A, et al. (2009) Efficacy of systemic morpholino exon-skipping in Duchenne dystrophy dogs. Ann Neurol 65: 667–676.
7. Sharp N, Kornegay J, Van Camp S, Herbstreith M, Secore S, et al. (1992) An error in dystrophin mRNA processing in golden retriever muscular dystrophy, an animal homologue of Duchenne muscular dystrophy. Genomics 13: 115–121.
8. Béroud C, Tuffery-Giraud S, Matsuo M, Hamroun D, Humbertclaude V, et al. (2007) Multiexon skipping leading to an artificial DMD protein lacking amino acids from exons 45 through 55 could rescue up to 63% of patients with Duchenne muscular dystrophy. Hum Mutat 28: 196–202.
9. Wee K, Pramono Z, Wang J, MacDorman K, Lai P, et al. (2008) Dynamics of co-transcriptional pre-mRNA folding influences the induction of dystrophin exon skipping by antisense oligonucleotides. PLoS ONE 3: e1844.
10. Pramono Z, Takeshima Y, Alimsardjono H, Ishii A, Takeda S, et al. (1996) Induction of exon skipping of the dystrophin transcript in lymphoblastoid cells by transfecting an antisense oligodeoxynucleotide complementary to an exon recognition sequence. Biochem Biophys Res Commun 226: 445–449.
11. Chelly J, Gilgenkrantz H, Hugnot J, Hamard G, Lambert M, et al. (1991) Illegitimate transcription. Application to the analysis of truncated transcripts of the dystrophin gene in nonmuscle cultured cells from Duchenne and Becker patients. J Clin Invest 88: 1161–1166.
12. Aartsma-Rus A, Janson A, Kaman W, Bremmer-Bout M, den Dunnen J, et al. (2003) Therapeutic antisense-induced exon skipping in cultured muscle cells from six different DMD patients. Hum Mol Genet 12: 907–914.
13. Aartsma-Rus A, Janson A, Kaman W, Bremmer-Bout M, van Ommen G, et al. (2004) Antisense-induced multiexon skipping for Duchenne muscular dystrophy makes more sense. Am J Hum Genet 74: 83–92.
14. Gonçalves M, Swildens J, Holkers M, Narain A, van Nierop G, et al. (2008) Genetic complementation of human muscle cells via directed stem cell fusion. Mol Ther 16: 741–748.
15. Cooper S, Kizana E, Yates J, Lo H, Yang N, et al. (2007) Dystrophinopathy carrier determination and detection of protein deficiencies in muscular dystrophy using lentiviral MyoD-forced myogenesis. Neuromuscul Disord 17: 276–284.
16. Zheng J, Wang Y, Karandikar A, Wang Q, Gai H, et al. (2006) Skeletal myogenesis by human embryonic stem cells. Cell Res 16: 713–722.
17. McClorey G, Moulton H, Iversen P, Fletcher S, Wilton S (2006) Antisense oligonucleotide-induced exon skipping restores dystrophin expression in vitro in a canine model of DMD. Gene Ther 13: 1373–1381.
18. Reiss J, Reininsland F (1994) An explanation for the constitutive exon 9 cassette splicing of the DMD gene. Hum Mol Genet 3: 295–298.
19. Miller A, Buttimore C (1986) Redesign of retrovirus packaging cell lines to avoid recombination leading to helper virus production. Mol Cell Biol 6: 2895–2902.
20. Morgenstern J, Land H (1990) A series of mammalian expression vectors and characterisation of their expression of a reporter gene in stably and transiently transfected cells. Nucleic Acids Res 18: 1068.
21. Choi J, Costa M, Mermelstein C, Chagas C, Holtzer S, et al. (1990) MyoD converts primary dermal fibroblasts, chondroblasts, smooth muscle, and retinal pigmented epithelial cells into striated mononucleated myoblasts and multinucleated myotubes. Proc Natl Acad Sci U S A 87: 7988–7992.
22. Etzion S, Barbash I, Feinberg M, Zarin P, Miller L, et al. (2002) Cellular cardiomyoplasty of cardiac fibroblasts by adenoviral delivery of MyoD ex vivo: an unlimited source of cells for myocardial repair. Circulation 106: I125–130.
23. Noda T, Fujino T, Mie M, Kobatake E (2009) Transduction of MyoD protein into myoblasts induces myogenic differentiation without addition of protein transduction domain. Biochem Biophys Res Commun 382: 473–477.
24. Shimatsu Y, Yoshimura M, Yuasa K, Urasawa N, Tomohiro M, et al. (2005) Major clinical and histopathological characteristics of canine X-linked muscular dystrophy in Japan, CXMDJ. Acta Myol 24: 145–154.
25. Mitrpant C, Adams A, Meloni P, Muntoni F, Fletcher S, et al. (2009) Rational design of antisense oligomers to induce dystrophin exon skipping. Mol Ther 17: 1418–1426.
26. Aartsma-Rus A, Kaman W, Weij R, den Dunnen J, van Ommen G, et al. (2006) Exploring the frontiers of therapeutic exon skipping for Duchenne muscular dystrophy by double targeting within one or multiple exons. Mol Ther 14: 401–407.
27. Harding P, Fall A, Honeyman K, Fletcher S, Wilton S (2007) The influence of antisense oligonucleotide length on dystrophin exon skipping. Mol Ther 15: 157–166.
28. Aartsma-Rus A, van Ommen G (2007) Antisense-mediated exon skipping: a versatile tool with therapeutic and research applications. RNA 13: 1609–1624.
29. Wilton S, Fall A, Harding P, McClorey G, Coleman C, et al. (2007) Antisense oligonucleotide-induced exon skipping across the human dystrophin gene transcript. Mol Ther 15: 1288–1296.
30. McClorey G, Fall A, Moulton H, Iversen P, Rasko J, et al. (2006) Induced dystrophin exon skipping in human muscle explants. Neuromuscul Disord 16: 583–590.
31. Aartsma-Rus A, De Winter C, Janson A, Kaman W, Van Ommen G, et al. (2005) Functional analysis of 114 exon-internal AONs for targeted DMD exon skipping: indication for steric hindrance of SR protein binding sites. Oligonucleotides 15: 284–297.
32. Hallegger M, Llorian M, Smith C (2010) Alternative splicing: global insights. FEBS J 277: 856–866.
33. Sironi M, Cagliani R, Pozzoli U, Bardoni A, Comi G, et al. (2002) The dystrophin gene is alternatively spliced throughout its coding sequence. FEBS Lett 517: 163–166.
34. Pruitt K, Harrow J, Harte R, Wallin C, Diekhans M, et al. (2009) The consensus coding sequence (CCDS) project: Identifying a common protein-coding gene set for the human and mouse genomes. Genome Res 19: 1316–1323.
35. Desmet F, Hamroun D, Lalande M, Collod-Béroud G, Claustres M, et al. (2009) Human Splicing Finder: an online bioinformatics tool to predict splicing signals. Nucleic Acids Res 37: e67.

Efficient gene transfer into neurons in monkey brain by adeno-associated virus 8

Yoshito Masamizu[a], Takashi Okada[b], Hidetoshi Ishibashi[a], Shin'ichi Takeda[b], Shigeki Yuasa[c] and Kiyoshi Nakahara[a,d]

Although the adeno-associated virus (AAV) vector is a promising tool for gene transfer into neurons, especially for therapeutic purposes, neurotropism in primate brains is not fully elucidated for specific AAV serotypes. Here, we injected AAV serotype 8 (AAV8) vector carrying the enhanced green fluorescent protein (EGFP) gene under a ubiquitous promoter into the cerebral cortex, striatum and substantia nigra of common marmosets. Robust neuronal EGFP expression was observed at all injected sites. Cell typing with immunohistochemistry confirmed efficient AAV8-mediated gene transfer into the pyramidal neurons in the cortex, calbindin-positive medium spiny neurons in the striatum and dopaminergic neurons in the substantia nigra. The results indicate a preferential tropism of AAV8 for subsets of neurons, but not for glia, in monkey brains. *NeuroReport* **21:447–451 © 2010 Wolters Kluwer Health | Lippincott Williams & Wilkins.**

NeuroReport 2010, 21:447–451

Keywords: adeno-associated virus, gene transfer, marmoset, motor cortex, neuron, nonhuman primate, striatum, substantia nigra, tropism

[a]Department of Animal Models for Human Disease, [b]Department of Molecular Therapy, [c]Department of Ultrastructural Research, National Institute of Neuroscience, NCNP and [d]PRESTO, Japan Science and Technology Agency

Correspondence to Dr Kiyoshi Nakahara, Department of Animal Models for Human Disease, National Institute of Neuroscience, NCNP, 4-1-1 Ogawa-Higashi, Kodaira, Tokyo 187-8502, Japan
Tel: +81 42 346 1724; fax: +81 42 346 1754; e-mail: nakahara@ncnp.go.jp

Received 24 January 2010 accepted 14 February 2010

Introduction

Adeno-associated virus (AAV) vectors are promising as a means to deliver genes into a wide range of tissues *in vivo*. They are eligible as gene therapy vectors, as qualified by their nonpathogenicity and long-term gene expression, and are particularly suitable for gene transfer into neurons of the central nervous system (CNS) because of their ability to infect nondividing cells [1,2]. In addition to their therapeutic applications, AAV-mediated gene transfer into the CNS is becoming increasingly valuable in basic neurophysiological research, particularly with the advent of genetic methods for experimental manipulation of neuronal activities, such as optogenetics [3,4]. Extensive exploration of the neurotropism of AAV vectors in primate brains is thus prerequisite for application to the gene therapy of neurological disorders and to neurophysiological research.

One remarkable feature of AAV vectors is their wide variety of serotypes originating from the variation in the amino acid sequence of the capsid proteins. Infection efficiency and cell tropism of the AAV vectors are mainly determined by their serotypes, which can directly affect epitopes recognized by the host immune system and preference for the receptors used for cell entry [1]. This feature also offers researchers opportunities for selecting an appropriate AAV serotype according to their purposes and target cells. Although AAV serotype 2 (AAV2) has been the most commonly used in both clinical applications and basic research among at least 100 identified serotypes [1], recent studies have revealed the potential and advantages of other serotypes [1,5–8]. Among these, adeno-associated virus serotype 8 (AAV8) has attracted interest for its higher efficiency than AAV2 in transferring genes into CNS neurons [9]. However, neuronal tropism of AAV8 has mainly been investigated in rodent brains, and tropism of AAV8 for neuronal cell types in primate brains is not yet fully elucidated.

Here, we investigated tropism and gene transfer efficiency of AAV8 vector in the brain of a new world monkey, the common marmoset. More specifically, we explored the ability of AAV8 to deliver genes into projection neurons in the striatum and dopaminergic neurons in the substantia nigra. These neurons constitute functional circuits within the extrapyramidal system, playing pivotal roles not only in normal functions such as action selection, but also in the pathophysiology of various neurological disorders such as Parkinson's disease [10–13]. This study reveals strong neuronal tropism of AAV8, as identified by several markers for neuronal subtypes in the pyramidal and extrapyramidal systems of the primate brain.

Methods

Monkeys

Two laboratory-bred adult male common marmosets (*Callithrix jacchus*) were used. The animals were 59 months (weight, 325 g) and 62 months (weight, 358 g) of age at the start of the experiment. Animal experiments were conducted in accordance with the NIH guidelines for the care and use of laboratory animals, and with the guidelines approved by the ethics committee for primate research of the National Center of Neurology and Psychiatry, Japan.

0959-4965 © 2010 Wolters Kluwer Health | Lippincott Williams & Wilkins

DOI: 10.1097/WNR.0b013e328338ba00

Virus preparation

AAV8-enhanced green fluorescent protein (EGFP) virus production and purification was performed as described earlier [14,15]. The vector plasmid (pAAV-EGFP) contained EGFP cDNA and the woodchuck hepatitis virus post-transcriptional regulatory element (WPRE) under the control of the CAG promoter, a modified chicken β-actin promoter with a cytomegalovirus immediate early enhancer. The pAAV-EGFP vector was cotransfected with an AAV8 chimeric helper plasmid encoding the AAV2 rep gene and the AAV8 cap gene, and an adenoviral helper plasmid pAdeno [16], into HEK293 cells by calcium phosphate coprecipitation with the use of active gassing [15]. Cell suspensions were collected 72 h after transfection, and centrifuged at $300 \times g$ for 10 min. Cell pellets were resuspended in 30 ml of Tris-buffered saline [100 mM Tris–HCl (pH 8.0), 150 mM NaCl]. AAV8-EGFP virus was harvested by five cycles of freeze-thawing of the resuspended pellet. The crude viral lysate was initially concentrated by a brief two-tier CsCl gradient centrifugation for 3 h [17], and further purified by dual ion-exchange chromatography [14]. The final number of AAV8-EGFP virus particles was determined by quantitative polymerase chain reaction of DNase I-treated stocks with plasmid standards, and was 3.0×10^{13} vector genomes (vg)/ml.

Virus injections

All surgical procedures and AAV8-EGFP virus injections were performed under aseptic conditions. Animals were initially anesthetized with 0.1 ml ketamine (50 mg/ml, intramuscularly). Animals were then intubated and placed in a stereotaxic apparatus with anesthesia maintained using inhaled isoflurane (1.5–2.5% in oxygen). Pulse oxygen (SpO_2), heart rate, body temperature, end-tidal CO_2 ($EtCO_2$), O_2 (EtO_2), isoflurane (EtISO), and fraction of inspired CO_2 ($FiCO_2$), O_2 (FiO_2), and isoflurane (FiISO) were continuously monitored to judge the animal's condition. After injection of 0.07 ml cefovecin (80 mg/ml, intramuscularly) as an antibiotic, a stereotaxic small craniotomy (2–3 mm in diameter) was then made over the area of interest, and the underlying dura was slit to allow penetration by the virus-containing 10-μl Hamilton syringe connected to a 33 G (45°angle) needle. Virus solution (3 μl) was injected at a rate of 0.25 μl/min to each site. Injection sites were determined using the Stereotaxic Atlas of the Marmoset Brain with Immunohistochemical Architecture and MRI Images (by Yuasa S, Nakamura K and Kohsaka S, in press). As injection sites, we aimed at the primary motor cortex: anterior (A) 12.0 mm from the interaural line, lateral (L) 6.8 mm from the midline, and ventral (V) 2.5 mm from the brain surface [18], the striatum: A 12.0 mm, L 3.0 mm, and V 6.0 mm [19], and the substantia nigra: A 5.5 mm, L 2.5 mm, and V 11.7 mm [20]. After each injection, the needle was kept in place for an additional 15 min (motor cortex) or 5 min (striatum and substantia nigra), and then slowly withdrawn (2 mm/min). We then waited 4 weeks after the virus injection for EGFP expression to appear.

Immunohistochemistry

The procedures were as reported earlier [21], with slight modifications. Briefly, 4 weeks after AAV8-EGFP virus injection, the animals were deeply anesthetized by an intraperitoneal injection of sodium pentobarbital, and then perfused through the ascending aorta with 4% paraformaldehyde dissolved in 0.1 M phosphate-buffered saline (PBS, pH 7.4). The brains were sampled, and then postfixed at 4°C for 3 days with the same fixative. The fixed brains were embedded in 3% agar in PBS, and then sliced coronally into 100 μm sections with a Microslicer (DTK-3000, DOSAKA EM, Kyoto, Japan). Immunohistochemical stainings were performed on free-floating sections. After 1 h of preincubation with 10% normal goat serum at 4°C, sections were incubated with primary antibodies in PBS containing 2% Triton X-100 at 4°C overnight. Antibodies against the following neuronal or glial marker proteins were used: neuron-specific nuclear protein (NeuN; mouse IgG, 1:500; Cat. No. MAB377, Millipore, Billerica, Massachusetts, USA), nonphosphorylated neurofilament protein (NNF; mouse IgG, 1:1000; Cat. No. SMI-32R, Sternberger Monoclonals, Baltimore, Maryland, USA) [22], calbindin D-28k (rabbit IgG, 1:1000; Cat. No. CB38a, Swant, Bellinzona, Switzerland), tyrosine hydroxylase (TH; mouse IgG, 1:1000; Cat. No. T2928, Sigma-Aldrich, St. Louis, Missouri, USA), glial fibrillary acidic protein (GFAP; rabbit IgG, 1:200; Cat. No. Z0334, Dako, Glostrup, Denmark), and oligodendrocyte transcription factor 2 (Olig2; rabbit IgG, 1:2000; Cat. No. AB9610, Millipore). Sections were then rinsed eight times with PBS, and incubated with secondary antibodies in PBS at 4°C for 5 h. Appropriate secondary antibody [Alexa goat anti-mouse 594 IgG (1:500; Cat. No. A11005, Molecular Probes, Eugene, Oregon, USA), or Alexa goat anti-rabbit 594 IgG (1:500; Cat. No. A11012, Molecular Probes)] directed against the species in which the primary antibody was raised, was used in each case. Sections were then rinsed five times with PBS. The stained sections were mounted on glass slides with Fluoromount-G (Beckman Coulter, Fullerton, California, USA) and examined with a confocal laser-scanning microscope (LSM5 Pascal, Zeiss, Oberkochen, Germany). EGFP expression was directly observed through confocal fluorescence images.

Results

Neuronal tropism of AAV8 in the marmoset brain *in vivo*

We injected recombinant AAV8 vector carrying the EGFP gene under the control of CAG promoter (AAV8-EGFP) into the brains of two common marmosets. Stereotaxic virus injections were carried out aiming at the motor cortex, the striatum and the substantia nigra. Four weeks after the injections, intense EGFP fluorescence was

directly observed in numerous cell bodies and fibers around all injected sites, indicating efficient EGFP gene transfer by the infection of AAV8-EGFP (Figs 1 and 2). As the CAG promoter has strong and ubiquitous activity, the types of EGFP-expressing ($EGFP^+$) cells would reflect endogenous tropism of AAV8 in the primate brain. Thus, we examined the tropism of AAV8-EGFP by immunostaining for neuronal or glial marker proteins. Confocal microscopic observations revealed that almost all of the $EGFP^+$ cells in the striatum were colocalized with NeuN (Fig. 1a–c). In contrast, the $EGFP^+$ cells were rarely colocalized with GFAP, or with Olig2, marker proteins for astrocytes and oligodendrocytes, respectively (Fig. 1d–i). These results indicated tropism of AAV8 for neurons, but not for glia, in the primate brain.

Identification of AAV8-infected neuronal cell types

We further characterized the $EGFP^+$ neurons by immunostaining for several markers of neuronal subtypes. In the motor cortex, most of the $EGFP^+$ cells were pyramidal neurons, as revealed by the coexpression of NNF, a cytoskeletal protein found in a subset of pyramidal neurons (Fig. 2a–d). Overlaps of EGFP fluorescence and NNF expression were evident in the apical dendrites (Fig. 2d). In the striatum, the $EGFP^+$ cells exhibited morphology characteristic of medium spiny neurons, the principal cell type in this region. Indeed, immunostaining confirmed that the majority of the $EGFP^+$ cells coexpressed calbindin, a specific marker for the medium spiny neuron [23] (Fig. 2e–h). We also found colocalization of EGFP fluorescence and TH immunoreactivity, a specific marker for dopaminergic neurons, in the substantia nigra (Fig. 2i–l).

Quantification of AAV8 infection efficiency in the identified neuronal cell types

Finally, to quantify the neuronal tropism of AAV8, we counted colocalizations of EGFP fluorescence and immunohistochemical staining of neuronal or glial marker proteins in the three injected regions ($n = 2$, Table 1). The majority of the $EGFP^+$ cells were colocalized with neuronal marker proteins, and the estimated percentages of colocalization were extremely high: 91% of the $EGFP^+$ cells colocalized with NNF in the motor cortex, 70% with calbindin in the striatum, and 99% with TH in the substantia nigra pars compacta. In the striatum, we also counted colocalizations of EGFP signal with NeuN, and the estimated percentage of colocalization reached 98%. In contrast, we hardly detected colocalization of the $EGFP^+$ cells with GFAP or with Olig2 in the three brain regions examined (3% or below).

Discussion

In this study, we injected AAV8-EGFP into three brain regions, the motor cortex, the striatum and the substantia nigra of two common marmosets. Almost all of the

Fig. 1

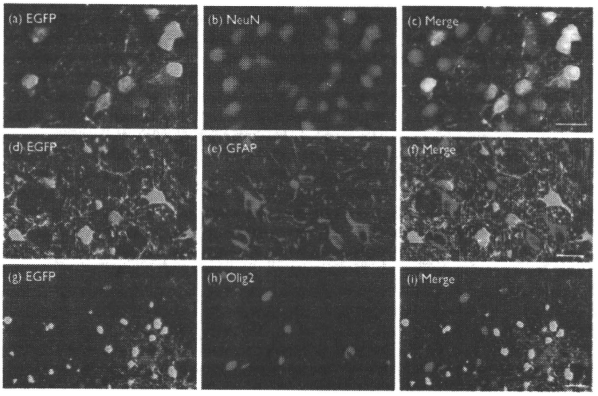

Adeno-associated virus serotype 8 preferentially transfers the enhanced green fluorescent protein (EGFP) gene into neurons in the primate striatum *in vivo*. Confocal images show EGFP-positive ($EGFP^+$) cells in the striatum (a, d, g; green). $EGFP^+$ cells are colocalized with neuron-specific nuclear protein (NeuN, b; red) as shown by the merged image (c; yellow). $EGFP^+$ cells are rarely colocalized with glial fibrillary acidic protein (GFAP, e; red) or oligodendrocyte transcription factor 2 (Olig2, h; red) as shown by the merged images (f and i). Bars: 20 μm.

Fig. 2

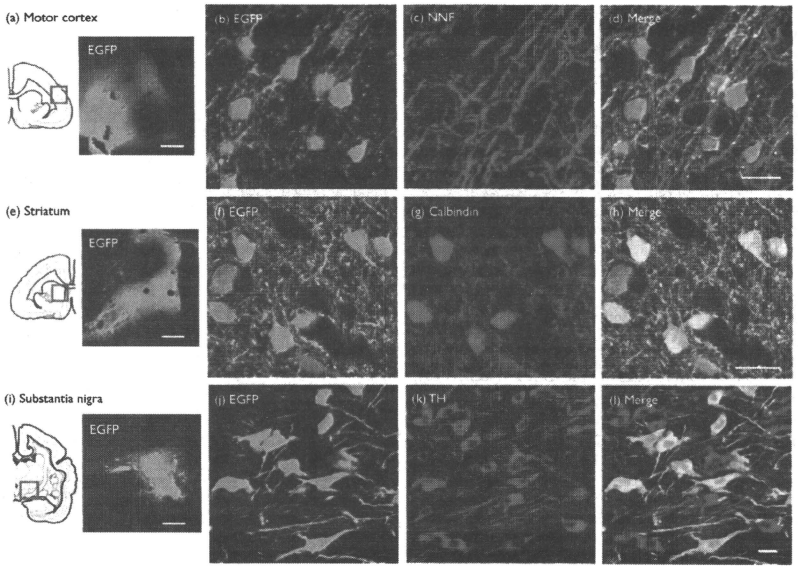

Identification of cell types of adeno-associated virus 8-infected neurons in the motor cortex, the striatum and the substantia nigra. Confocal images with a low-power field show native enhanced green fluorescent protein (EGFP) fluorescence at the three injection sites (a, e, i; green), approximately corresponding to the red boxes on the insets of coronal marmoset brain maps. High-power confocal images show EGFP$^+$ cells (green) in the motor cortex (b), the striatum (f) and the substantia nigra (j). EGFP$^+$ cells are colocalized with non-phosphorylated neurofilament protein (NNF, c; red), calbindin (g; red), and tyrosine hydroxylase (TH, k; red) as shown by the merged images (d, h, l; yellow). Bars represent 500 μm in (a), (e), (i), and 20 μm in (d), (h), (l).

Table 1 Quantification of infection efficiency in identified neuronal cell types after AAV8-EGFP virus injection

Injection site	Neuron (neuronal marker$^+$/ EGFP$^+$cells)	Astrocyte (GFAP$^+$/ EGFP$^+$cells)	Oligodendrocyte (Olig2$^+$/ EGFP$^+$cells)
Motor cortex	91% (169/185)	1% (2/189)	0% (0/197)
Striatum	98% (190/193)a 70% (142/202)b	0% (0/195)	1% (2/207)
Substantia nigra pars compacta	99% (190/192)	0% (0/193)	3% (5/190)

NNF in the motor cortex, NeuN (a) and calbindin (b) in the striatum, and TH in the substantia nigra were used as the neuronal marker.
AAV, adeno-associated virus; EGFP, enhanced green fluorescence protein; GFAP, glial fibrillary acidic protein; NeuN, neuron-specific nuclear protein; NNF, nonphosphorylated neurofilament protein; Olig2, oligodendrocyte transcription factor 2; TH, tyrosine hydroxylase.

EGFP$^+$ cells in each injected site were colocalized with neuron-specific markers. In contrast, we rarely found colocalization of EGFP fluorescence with specific marker proteins for glial cells. As we used a ubiquitous promoter (CAG promoter) in this study, the present results indicate endogenous AAV8 tropism for neurons, but not for glia, in marmoset brains *in vivo*. The neuronal tropism of AAV8 revealed in the present study is consistent with an earlier study in cynomolgus monkeys [24]. It has been shown that AAV8 could transfect astroglia in primary culture prepared from newborn rats, but rarely *in vivo* in rat hippocampus [25]. Therefore, the degree of neurotropism of AAV8 may depend on the infection conditions (*in vivo* vs. *in vitro*).

In the present study, we examined EGFP expression 4 weeks after injection of AAV8-EGFP. Eslamboli *et al.* [20] showed long-term (at least 1 year) transgene expression through AAV5 in the marmoset substantia nigra. Thus, it is likely that AAV8 also enables stable transgene expression in primate brains for long periods.

One main goal of this study was to examine the ability of AAV8 to transfer foreign genes into identified neuronal cell types in primate brain. Specifically, we explored the ability of AAV8 to transfect projection neurons in the striatum and dopaminergic neurons in the substantia nigra, which constitute functional circuits within the nigrostriatal loop [10–13]. Clinically, dysfunctions of the basal ganglia circuit have been related to many neurological disorders including Parkinson's disease and Huntington's disease. AAV-mediated gene transfer is one of the most promising means for gene therapy of these diseases, and preclinical investigations of the tropism of AAV for functionally identified neurons are requisite steps for future practical applications. In this study, we successfully showed efficient AAV8 transfection of calbindin-positive neurons in the striatum and TH-positive dopaminergic neurons in the substantia nigra. These results indicate the potential of AAV8 vector as a therapeutic tool for basal ganglia-related diseases. Other than the therapeutic applications, AAV8 will be useful to deliver molecular tools to experimentally monitor or manipulate neuronal activities in primate brains [3,4]. Further research is needed to clarify the infection spectrum of AAV8 and other AAV serotypes in many other neuronal cell types in the primate brain.

Conclusion

AAV8 vector has strong tropism for neurons but not for glia in the brain of the common marmoset *in vivo*. Efficient AAV8-mediated gene transfer into identified neuronal cell types, calbindin-positive medium spiny neurons in the striatum and TH-positive dopaminergic neurons in the substantia nigra, was also successfully shown.

Acknowledgements

This work was supported by a JSPS Research Fellowship for Young Scientists (Y.M.), and by PRESTO, JST (K.N.). All the authors declare that they have no conflict of interest.

References

1 Daya S, Berns KI. Gene therapy using adeno-associated virus vectors. *Clin Microbiol Rev* 2008; **21**:583–593.
2 Kaplitt MG, Leone P, Samulski RJ, Xiao X, Pfaff DW, O'Malley KL, *et al.* Long-term gene expression and phenotypic correction using adeno-associated virus vectors in the mammalian brain. *Nat Genet* 1994; **8**:148–154.
3 Zhang F, Aravanis AM, Adamantidis A, de Lecea L, Deisseroth K. Circuit-breakers: optical technologies for probing neural signals and systems. *Nat Rev Neurosci* 2007; **8**:577–581.
4 Han X, Qian X, Bernstein JG, Zhou HH, Franzesi GT, Stern P, *et al.* Millisecond-timescale optical control of neural dynamics in the nonhuman primate brain. *Neuron* 2009; **62**:191–198.
5 Ohshima S, Shin JH, Yuasa K, Nishiyama A, Kira J, Okada T, *et al.* Transduction efficiency and immune response associated with the administration of AAV8 vector into dog skeletal muscle. *Mol Ther* 2009; **17**:73–80.
6 Zincarelli C, Soltys S, Rengo G, Rabinowitz JE. Analysis of AAV serotypes 1-9 mediated gene expression and tropism in mice after systemic injection. *Mol Ther* 2008; **16**:1073–1080.
7 Gao GP, Alvira MR, Wang L, Calcedo R, Johnston J, Wilson JM. Novel adeno-associated viruses from rhesus monkeys as vectors for human gene therapy. *Proc Natl Acad Sci U S A* 2002; **99**:11854–11859.
8 Rutledge EA, Halbert CL, Russell DW. Infectious clones and vectors derived from adeno-associated virus (AAV) serotypes other than AAV type 2. *J Virol* 1998; **72**:309–319.
9 Broekman ML, Comer LA, Hyman BT, Sena-Esteves M. Adeno-associated virus vectors serotyped with AAV8 capsid are more efficient than AAV-1 or -2 serotypes for widespread gene delivery to the neonatal mouse brain. *Neuroscience* 2006; **138**:501–510.
10 Nicola SM, Surmeier J, Malenka RC. Dopaminergic modulation of neuronal excitability in the striatum and nucleus accumbens. *Annu Rev Neurosci* 2000; **23**:185–215.
11 Nambu A, Tokuno H, Takada M. Functional significance of the cortico-subthalamo-pallidal, hyperdirect, pathway. *Neurosci Res* 2002; **43**:111–117.
12 Redgrave P, Gurney K. The short-latency dopamine signal: a role in discovering novel actions? *Nat Rev Neurosci* 2006; **7**:967–975.
13 Obeso JA, Marin C, Rodriguez-Oroz C, Blesa J, Benitez-Temino B, Mena-Segovia J, *et al.* The basal ganglia in Parkinson's disease: current concepts and unexplained observations. *Ann Neurol* 2008; **64 (Suppl 2)**:S30–S46.
14 Okada T, Nonaka-Sarukawa M, Uchibori R, Kinoshita K, Hayashita-Kinoh H, Nitahara-Kasahara Y, *et al.* Scalable purification of adeno-associated virus serotype 1 (AAV1) and AAV8 vectors, using dual ion-exchange adsorptive membranes. *Hum Gene Ther* 2009; **20**:1013–1021.
15 Okada T, Nomoto T, Yoshioka T, Nonaka-Sarukawa M, Ito T, Ogura T, *et al.* Large-scale production of recombinant viruses by use of a large culture vessel with active gassing. *Hum Gene Ther* 2005; **16**:1212–1218.
16 Matsushita T, Elliger S, Elliger C, Podsakoff G, Villarreal L, Kurtzman GJ, *et al.* Adeno-associated virus vectors can be efficiently produced without helper virus. *Gene Ther* 1998; **5**:938–945.
17 Okada T, Shimazaki K, Nomoto T, Matsushita T, Mizukami H, Urabe M, *et al.* Adeno-associated viral vector-mediated gene therapy of ischemia-induced neuronal death. *Methods Enzymol* 2002; **346**:378–393.
18 Burman KJ, Palmer SM, Gamberini M, Spitzer MW, Rosa MG. Anatomical and physiological definition of the motor cortex of the marmoset monkey. *J Comp Neurol* 2006; **506**:860–876.
19 Eslamboli A, Georgievska B, Ridley RM, Baker HF, Muzyczka N, Burger C, *et al.* Continuous low-level glial cell line-derived neurotrophic factor delivery using recombinant adeno-associated viral vectors provides neuroprotection and induces behavioral recovery in a primate model of Parkinson's disease. *J Neurosci* 2005; **25**:769–777.
20 Eslamboli A, Romero-Ramos M, Burger C, Bjorklund T, Muzyczka N, Mandel RJ, *et al.* Long-term consequences of human alpha-synuclein overexpression in the primate ventral midbrain. *Brain* 2007; **130**:799–815.
21 Nakahira E, Yuasa S. Neuronal generation, migration, and differentiation in the mouse hippocampal primordium as revealed by enhanced green fluorescent protein gene transfer by means of in utero electroporation. *J Comp Neurol* 2005; **483**:329–340.
22 Bourne JA, Warner CE, Rosa MG. Topographic and laminar maturation of striate cortex in early postnatal marmoset monkeys, as revealed by neurofilament immunohistochemistry. *Cereb Cortex* 2005; **15**:740–748.
23 Parent A, Fortin M, Cote PY, Cicchetti F. Calcium-binding proteins in primate basal ganglia. *Neurosci Res* 1996; **25**:309–334.
24 Dodiya HB, Bjorklund T, Stansell Iii J, Mandel RJ, Kirik D, Kordower JH. Differential transduction following basal ganglia administration of distinct pseudotyped AAV capsid serotypes in nonhuman primates. *Mol Ther* 2009; doi:10.1038/mt.2009.216.
25 Klein RL, Dayton RD, Leidenheimer NJ, Jansen K, Golde TE, Zweig RM. Efficient neuronal gene transfer with AAV8 leads to neurotoxic levels of tau or green fluorescent proteins. *Mol Ther* 2006; **13**:517–527.

EXPERIMENTAL CELL RESEARCH 316 (2010) 2932–2944

available at www.sciencedirect.com

ScienceDirect

www.elsevier.com/locate/yexcr

Research Article

Six family genes control the proliferation and differentiation of muscle satellite cells

Hiroshi Yajima[a], *Norio Motohashi*[b], *Yusuke Ono*[b], *Shigeru Sato*[a], *Keiko Ikeda*[a], *Satoru Masuda*[b], *Erica Yada*[b], *Hironori Kanesaki*[b], *Yuko Miyagoe-Suzuki*[b], *Shin'ichi Takeda*[b], *Kiyoshi Kawakami*[a,*]

[a]*Division of Biology, Center for Molecular Medicine, Jichi Medical University, Tochigi, Japan*
[b]*Department of Molecular Therapy, National Institute of Neuroscience, National Center of Neurology and Psychiatry, Tokyo, Japan*

ARTICLE INFORMATION

Article Chronology:
Received 1 April 2010
Revised version received 19 July 2010
Accepted 3 August 2010
Available online 6 August 2010

Keywords:
Muscle satellite cell
Six gene
Cell proliferation
Muscle differentiation
Retrovirus-mediated overexpression
Gene knockdown

ABSTRACT

Muscle satellite cells are essential for muscle growth and regeneration and their morphology, behavior and gene expression have been extensively studied. However, the mechanisms involved in their proliferation and differentiation remain elusive. Six1 and Six4 proteins were expressed in the nuclei of myofibers of adult mice and the numbers of myoblasts positive for Six1 and Six4 increased during regeneration of skeletal muscles. Six1 and Six4 were expressed in quiescent, activated and differentiated muscle satellite cells isolated from adult skeletal muscle. Overexpression of *Six4* and *Six5* repressed the proliferation and differentiation of satellite cells. Conversely, knockdown of Six5 resulted in augmented proliferation, and that of Six4 inhibited differentiation. Muscle satellite cells isolated from $Six4^{+/-}Six5^{-/-}$ mice proliferated to higher cell density though their differentiation was not altered. Meanwhile, overproduction of Six1 repressed proliferation and promoted differentiation of satellite cells. In addition, Six4 and Six5 repressed, while Six1 activated *myogenin* expression, suggesting that the differential regulation of *myogenin* expression is responsible for the differential effects of *Six* genes. The results indicated the involvement of *Six* genes in the behavior of satellite cells and identified *Six* genes as potential target for manipulation of proliferation and differentiation of muscle satellite cells for therapeutic applications.

Introduction

Muscle satellite cells are tissue-specific stem cells that reside beneath the basal lamina surrounding the myofibers of mature adult skeletal muscles and play a major role in post-natal muscle growth and regeneration [1, for review see 2]. In the intact adult muscles, satellite cells are mitotically quiescent, while in the injured or damaged muscle, they are activated to proliferate, differentiate and then regenerate myofibers by fusing with each other or with residual fibers. The recent discovery of specific markers for muscle satellite cells, including Pax7, M-cadherin, MyoD and myogenin, has allowed the identification of the status of these cells [2]. Pax7 and M-cadherin is expressed in quiescent satellite cells, while MyoD is rapidly induced during activation of satellite cells [3]. The Pax7- and MyoD-double-positive cells are regarded as transit amplifying cells and future myoblasts [3]. It is

* *Corresponding author.* Division of Biology, Center for Molecular Medicine, Jichi Medical University, 3311-1, Yakushiji, Shimotsuke, Tochigi, 329-0498, Japan. Fax: +81 285 44 5476.
E-mail address: kkawakam@jichi.ac.jp (K. Kawakami).

0014-4827/$ – see front matter © 2010 Elsevier Inc. All rights reserved.
doi:10.1016/j.yexcr.2010.08.001

noted that some transit amplifying cells become MyoD-negative, and those are thought to re-enter the quiescent state [3]. The expression of Pax7 is down-regulated before commitment to terminal differentiation. Despite such progress in our understanding of the lineage and behavior of muscle satellite cells, there are other areas that remain poorly understood; for example, the exact mechanism that orchestrates the proliferation and differentiation of these cells.

Recently, we developed a new and efficient method to isolate quiescent satellite cells using monoclonal antibody SM/C-2.6 [4]. SM/C-2.6-positive cells co-express M-cadherin and become MyoD-positive in growth media. They are differentiated into desmin- and MyoD-positive myofibers under differentiation conditions. In the same study, we showed that the sorted muscle satellite cells differentiated into muscle fibers following their injection into *mdx* mouse muscles [4]. Furthermore, genome-wide gene expression analysis using the isolated cells allowed the identification of a quiescent cell-specific marker, calcitonin receptor (CTR), implicating the involvement of calcitonin/CTR signaling in the activation of satellite cells [5]. Thus, the SM/C-2.6-positive satellite cells are useful tool for investigating the mechanism of regulation of proliferation and differentiation *in vitro* and allow us to gain a better understanding of the role of satellite cells during muscle regeneration, compared to the use of cell lines such as C2C12 and MM14 cells.

The *Six* genes have been identified as homologues of *Drosophila sine oculis*, which is crucial for compound-eye formation [6,7]. The mammalian *Six* gene family consists of six members, *Six1* to *Six6* [8]. During development, *Six1* and *Six4* play important roles in the formation of various organs, such as olfactory epithelium, cranial ganglia, inner ear, kidney, skeletal muscle and skeleton [9–20]. During skeletal muscle development, *Six1* and *Six4* are expressed in the somite and migrating myoblasts and play important roles in myogenesis [21–23]. Another member of the *Six* gene family, *Six5*, is expressed in the somite and adult skeletal muscles [22,24,25]. Genetic ablation of both *Six1* and *Six4* results in gross muscle hypoplasia [21]. Limb muscles derived from hypaxial progenitors disappear, as a result of aberrant migration and apoptosis of myoblasts, which are caused by down-regulation of Pax3. Epaxial and other hypaxial muscles are impaired through severely compromised expression of myogenic regulatory factors (MRF) genes, Mrf4 and myogenin, within the myotome [21]. Expression of myogenin is thought to be directly controlled by Six1, Six4 and Six5 via MEF3 sites *in vivo* [26] and in cultured cells [27]. Moreover, *Six1* and *Six4* are necessary for the induction of the fast-type-muscle program during myogenesis [23] and are involved in the assignment of the fast/glycolytic character of the myofiber in adult skeletal muscles [22]. However, there is virtually no information on the role of *Six1*, *Six4* and *Six5* in muscle regeneration, especially in the proliferation and differentiation of muscle satellite cells.

In the present study, we analyzed the expression of *Six1*, *Six4* and *Six5* in adult skeletal muscles during regeneration and in satellite cells *in vivo* and in culture. We examined the effects of overexpression and knockdown of *Six* genes on the proliferation and differentiation of isolated satellite cells *in vitro*. Finally, the proliferation and differentiation of muscle satellite cells isolated from *Six4*- and *Six5*-deficient mice were compared to those of wild-type mice. The results demonstrated the involvement of *Six* genes in the regulation of proliferation and differentiation of muscle satellite cells.

Results

Induction of expression of Six proteins during regeneration of adult skeletal muscle

To investigate the expression of *Six* genes during skeletal muscle regeneration, we induced muscle damage by injecting cardiotoxin into the tibialis anterior (TA) muscles of 8- to 12-week-old wild-type mice. Three days after the injection, transverse sections of TA muscles were prepared from the injected as well as intact mice and mapped the distribution of Six proteins by immunofluorescence using specific antibodies to Six1 and Six4 [10,18]. In the intact non-injected TA muscles, a considerable number of muscle nuclei was positive for Six1 (Fig. 1A). The Six1-positive nuclei were located inside the muscle basal laminae, which were visualized by immunofluorescence using anti-laminin antibody (Figs. 1B and C). This indicates that the nuclei of the myofibers are positive for Six1 in the adult skeletal muscle. Most of the Six1-positive nuclei were also positive for Six4 (Figs. 1D–F). In the regenerating TA muscle, the number of cells positive for Six1 was far greater than that of control TA muscle (Fig. 1I, compare to 1A). The Six1-positive cells in the regenerating TA muscle were located inside and outside the basal laminae (Figs. 1J and K). As observed in the control TA muscles, most of the cells positive for Six1 were also positive for Six4 in the regenerating TA muscle (Figs. 1L–N). It was noted that the relative intensities of immunofluorescent signals for Six1 and Six4 were more variable in the regenerating muscle (Fig. 1N), compared to those in the intact muscle (Fig. 1F). To determine the type of cells positive for Six1 and Six4, we examined the expression of MyoD, a marker of proliferating myogenic precursor cells and postmitotic myocytes in the regenerating muscle [28–30]. Triple immunofluorescence using anti-Six1, anti-Six4 and anti-MyoD antibodies revealed that most of the immunofluorescent signals of Six1 and Six4 were colocalized with that of MyoD (Figs. 1O and P). As shown in Fig. 1Q, $90.1 \pm 0.42\%$ of Six1-positive cells and $91.7 \pm 1.06\%$ of Six4-positive cells were colocalized with MyoD. Moreover, remarkable amounts of Six1 and Six4 immunofluorescent signals were positive for Ki67, a marker of proliferating cells, suggesting that substantial populations of Six1- and Six4-positive cells were mitotic (Figs. 1R–T, data not shown). Colocalization of Six1 and Six4 with MyoD was not observed in the control skeletal muscle (Figs. 1G and H). These findings indicate that (i) Six1 and Six4 are expressed both in normal and regenerating muscles and (ii) the number of cells positive for Six1 and Six4 robustly increases during regeneration of adult skeletal muscle and many of them are proliferating myogenic precursors.

Expression of Six proteins in muscle satellite cells

In the adult skeletal muscle, typical quiescent satellite cells can be recognized as mononuclear cells beneath the basal lamina, and these cells are positive for both Pax7 and M-cadherin [30–32]. To determine whether Six proteins are expressed in quiescent muscle satellite cells, we performed immunofluorescence studies for Six1, Pax7 and M-cadherin. Immunofluorescent signals of Pax7 (Fig. 2A) and M-cadherin (Fig. 2B) were observed in the mononuclear cells of adult TA muscle (Figs. 2A, B and E, arrowheads and insets). Six1 immunofluorescence signal was also observed in these cells

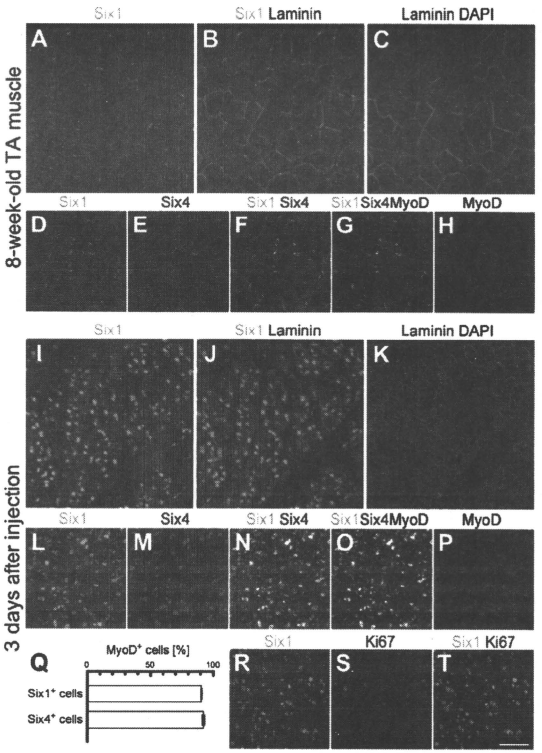

Fig. 1 – Expression of Six1 and Six4 in regenerating skeletal muscles of adult mice. (A–C) Cross-sections of intact TA muscle of 8-week-old mouse were stained with antibodies to Six1 (green) and laminin (red). Nuclei were stained with DAPI (blue). Note the subset of nuclei beneath the laminin layer is positive for Six1. (D–H) Immunofluorescence of cross-sections of TA muscle immunostained with antibodies for Six1 (green), Six4 (red) and MyoD (blue). Merged figures are shown in panels F and G. Most Six1-positive nuclei were positive for Six4 (E and F). MyoD was not detected in the adult TA muscle (H). (I–K) Cross-sections of regenerating TA muscle 3 days after cardiotoxin injection were co-immunostained with antibodies to Six1 (green) and laminin (red). Nuclei were stained with DAPI (blue). Note Six1-positive nuclei located inside and outside the laminin layer (J). (L–P) Immunofluorescence of cross-sections of regenerating TA muscle immunostained with antibodies for Six1 (green), Six4 (red) and MyoD (blue). Merged figures are shown in panels N and O. The majority of Six1-positive nuclei are also positive for Six4. Most of Six1- and Six4-positive nuclei are colocalized with MyoD. The percentages of MyoD-positive cells were quantified in (Q). Data are mean ± SEM. (R–T) Regenerating TA muscle immunostained with antibodies for Six1 (green) and Ki67 (red). A remarkable number of Six1-positive nuclei is positive for mitotic marker, Ki67. Scale bar: 50 μm.

(Figs. 2C and D, arrowheads and insets). The expression of Six4 was also observed in the satellite cells positive for M-cadherin in the adult TA muscle (Fig. 2F, thick arrow and inset). It is noteworthy that some of the nuclei within the myofibers, which were negative for Pax7 and M-cadherin, were positive for Six1 and Six4 (Figs. 2C–F arrows, data not shown). Vice versa, some of the Pax7 and M-cadherin-positive cells were negative for Six1 and Six4 (data not shown).

To examine the expression of Six proteins in muscle satellite cells during activation, proliferation and differentiation, we isolated and cultured satellite cells from limb and back muscles of wild-type mice by FACS technique using the monoclonal antibody SM/C-2.6 [4,5]

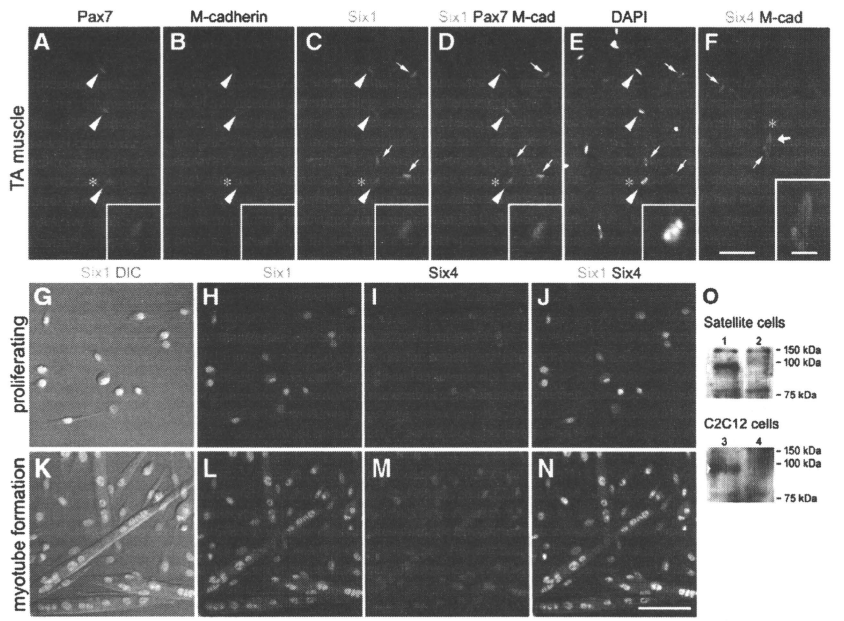

Fig. 2 – Six1, Six4 and Six5 are expressed in muscle satellite cells. (A–F) Cross-sections of TA muscle of 8-week-old mouse were immunostained with antibodies to Pax7 (red in A), M-cadherin (blue in B) and Six1 (green in C). Merged figures are shown in (D). The position of nuclei was visualized with DAPI, as shown in panel E. Satellite cells were labeled with the co-immunofluorescence of both Pax7 and M-cadherin (arrowheads). A subset of Six1-positive cells was satellite cells (C and D). A subset of Six4-positive cells was also labeled with M-cadherin (thick arrow in F). Arrows indicate myonuclei positive for Six1 or Six4 (C–F). Insets show close-up of satellite cells (labeled by asterisk). (G–N) Immunofluorescence of SM/C-2.6-positive satellite cells in the growth medium (G–J) or in the differentiation medium (K–N) using antibodies to Six1 (G, H, K and L in green) and Six4 (I and M in red). Merged figures are shown in panels J and N. Differential interference contrast (DIC) image showed that the majority of satellite cells were mononuclear fibroblastic cells in the growth medium (G) or formed multinucleated myotubes in the differentiation medium (K). Cultured satellite cells were positive for both Six1 and Six4 (J and N). Scale bars: 20 μm (A–F), 5 μm (insets) and 100 μm (G–N). (O) Nuclear (lane 1) and cytoplasmic (lane 2) extracts from SM/C-2.6-positive satellite cells were analyzed by western blotting with anti-Six5 antibody. For reference, nuclear (lane 3) and cytoplasmic (lane 4) extracts were also prepared from C2C12 cells and analyzed. Arrowheads indicate the positions of the detected Six5 proteins. The position of molecular mass marker is shown on the right.

and used immunofluorescence staining to check for the presence of Six1 and Six4. Six1 immunofluorescence was observed in virtually all muscle satellite cells in the growth medium (Figs. 2G and H). Six4 immunofluorescence was also observed in these satellite cells (Fig. 2I). Although Six1 and Six4 were colocalized in almost all satellite cells, the relative immunofluorescence intensity and subcellular distribution of Six1 and Six4 varied among individual cells (Fig. 2J). To examine whether Six1 and Six4 proteins are present during differentiation, the isolated satellite cells were cultured in the differentiation medium. Most of the satellite cells formed myotubes within 24 hours (Fig. 2K). Myonuclei in the myotubes were positive for Six1 (Figs. 2K and L) and Six4 (Fig. 2M), though the relative immunofluorescence intensities varied among myonuclei (Fig. 2N), as observed in the growth medium (Fig. 2J). We investigated the presence of Six5 in satellite cells by western blotting (Fig. 2O). Nuclear and cytoplasmic extracts from muscle satellite cells cultured in the growth medium were prepared and analyzed by western blotting using anti-Six5 antibody. Six5 protein was detected in nuclear extracts (Fig. 2O lane 1) but not in the cytoplasmic extracts (Fig. 2O lane 2). Furthermore, Six5 protein was detected in nuclear extracts only, but not cytoplasmic extracts, prepared from the control C2C12 mouse myoblast cell (Fig. 2O, lanes 3 and 4, respectively). These results indicate the presence of Six proteins mainly in the nuclei of quiescent, proliferating and differentiating muscle satellite cells.

Overexpression of Six genes inhibits proliferation of muscle satellite cells

Having shown that Six proteins are expressed in quiescent, proliferating and differentiating muscle satellite cells, we next investigated the effects of overexpression of *Six1* as well as *Six4* and *Six5* in isolated muscle satellite cells. In these studies, a retrovirus-mediated system [33] was used to overproduce Six1, Six4 and Six5 proteins. Six proteins and EGFP were connected by IRES. EGFP fluorescence was used to monitor cells transduced with the recombinant retrovirus. Accumulation of Six1, Six4 and Six5 proteins was noted in the nuclei of EGFP-positive cells after infection with a retrovirus harboring *Six1*, *Six4* or *Six5* cDNA, respectively (Supplementary Fig. 1). The nuclear localization was similar to the endogenous Six proteins both *in vivo* and *in vitro* (Figs. 1 and 2).

To analyze the effects of overexpression of *Six* genes on cell proliferation, we assessed the expression of proliferation markers, phospho-histone H3 and Ki67, by immunofluorescence (Fig. 3). Among the cells infected with the control retrovirus, a subset of EGFP-expressing cells was positive for phospho-histone H3 (Fig. 3A, arrowheads). In contrast, the signal of phospho-histone H3 was rarely observed in EGFP-positive cells infected with a retrovirus harboring *Six1*, *Six4* or *Six5* cDNA (Figs. 3B–D). Immunofluorescence of Ki67 was also observed in EGFP-positive cells infected with the control virus (Fig. 3E, arrowheads), but rarely in EGFP-positive cells infected with the retrovirus harboring *Six1*, *Six4* or *Six5* cDNA (Figs. 3F–H). To quantify cell proliferation, we determined the percentage of Ki67-positive cells among the EGFP-positive cells (Fig. 3I). The Ki67 index was $15.1 \pm 2.2\%$ in control, but significantly reduced to $5.7 \pm 1.4\%$, $4.8 \pm 1.9\%$ and $5.4 \pm 1.3\%$ in cells infected with retrovirus harboring *Six1*, *Six4* and *Six5*, respectively, indicating that overproduction of these Six proteins suppresses the proliferation of satellite cells.

Overexpression of Six1 promotes and excess Six4 and Six5 repress differentiation of muscle satellite cells

To investigate the effects of *Six* gene overexpression on the differentiation of muscle satellite cells, these cells were cultures in differentiation medium after retrovirus infection. EGFP signals were detected in myotubes and scattered mononuclear cells in the control experiment (Fig. 4A). Infection of the satellite cells with a retrovirus harboring *Six1* resulted in a considerable increase in the size of EGFP-positive myotubes relative to the control (Fig. 4B). On the other hand, many scattered single cells were positive for EGFP and fewer myotubes were observed when the retrovirus harboring *Six4* or *Six5* was used for infection (Figs. 4C and D). To assess cell differentiation, the fusion index of EGFP-positive cells (see Materials and methods) and the mean number of nuclei in EGFP/skeletal muscle myosin-double positive cells were determined after viral infection (Figs. 4E and F). The fusion index was $63.9 \pm 3.62\%$ in cells infected with the control retrovirus, and significantly higher ($82.3 \pm 2.39\%$) in cells infected with the retrovirus harboring *Six1* (Fig. 4E). In contrast, the index was $15.0 \pm 3.19\%$ and $13.8 \pm 2.72\%$ in Six4- and Six5-overexpressing cells, respectively; the latter values were significantly lower than the control. The mean number of nuclei in myosin-positive cells was 2.30 ± 0.20 when the control virus was used for infection (Fig. 4F), but increased to 3.82 ± 0.39 in cells infected with retrovirus harboring *Six1*, and decreased to 1.18 ± 0.06 and 1.16 ± 0.05 by infection with retrovirus overexpressing *Six4* and *Six5*, respectively. These results indicate that overproduction of Six1 stimulates while that of Six4 or Six5 inhibits the differentiation of muscle satellite cells in the differentiation medium.

To confirm the above effects of *Six* genes overexpression on satellite cell differentiation, the fusion index of EGFP-positive cells and the mean number of nuclei in myosin-positive cells were determined in the growth medium (Fig. 4G and H). The fusion

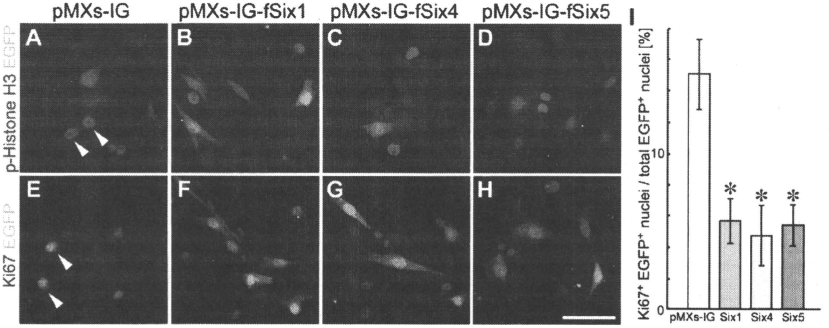

Fig. 3 – Overproduction of Six1, Six4 and Six5 interferes with proliferation of muscle satellite cells. Immunofluorescence of satellite cells infected with control retrovirus (A and E) or retrovirus harboring *Six1* (B and F), *Six4* (C and G) or *Six5* (D and H) in the growth medium using antibodies to phospho-histone H3 (A–D) or Ki67 (E–H), shown in red. Arrowheads point to EGFP-positive cells immunostained with anti-phospho-histone H3 (A) or anti-Ki67 (E) antibodies. Scale bar: 50 μm. (I) The percentages of Ki67-positive nuclei among EGFP-positive cells infected with control retrovirus (pMXs-IG) and retrovirus harboring *Six1* (Six1), *Six4* (Six4) or *Six5* (Six5) were calculated. Data are mean ± SEM of three independent cell isolates. *$p < 0.001$, compared with pMXs-IG.

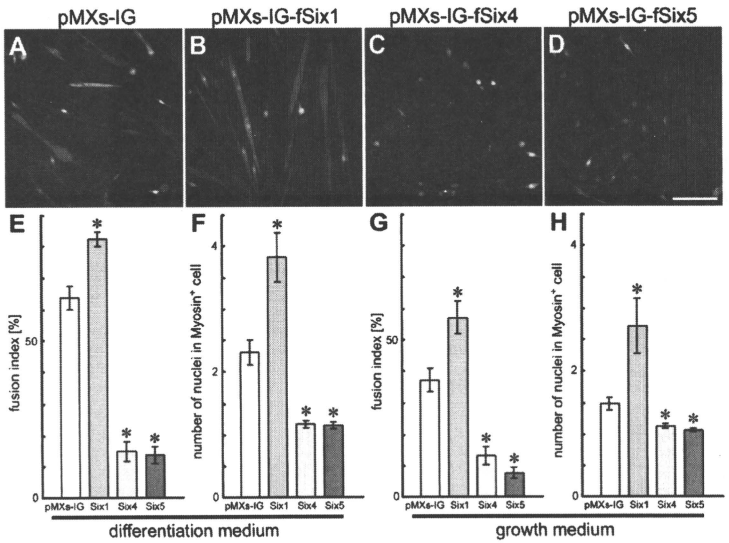

Fig. 4 – Effects of overproduction of Six1, Six4 and Six5 on differentiation of muscle satellite cells. Representative images of EGFP-positive cells infected with control retrovirus (A) and retrovirus harboring *Six1* (B), *Six4* (C) or *Six5* (D) in the differentiation medium. Nuclei were stained with DAPI (blue). Scale bar: 100 μm. The percentage of nuclei within myotubes (fusion index) was calculated among the EGFP-positive cells (E and G) and the number of nuclei in EGFP and skeletal muscle myosin-double positive cells was counted and averaged (F and H) in the differentiation medium or growth medium, respectively, following infection with control retrovirus (pMXs-IG) or retrovirus harboring *Six1* (Six1), *Six4* (Six4) or *Six5* (Six5). Data are mean ± SEM of three independent cell isolates. *$p < 0.001$, compared with pMXs-IG.

index was 37.2 ± 3.73% and the mean number of nuclei in myosin-positive cells was 1.48 ± 0.10 in cells infected with the control retrovirus (Figs. 4G and H, pMXs-IG). These observations clearly indicate that differentiation occurs in a subset of satellite cells even in the growth medium, although the extent of differentiation is lower than that in the differentiation medium. Infection with a retrovirus harboring *Six1* increased the fusion index to 57.3 ± 5.35% as well as the mean number of nuclei in myosin-positive cells to 2.72 ± 0.45. On the other hand, in cells infected with retrovirus harboring *Six4* or *Six5*, the fusion index and mean number of nuclei in myosin-positive cells were reduced to 13.3 ± 2.93% or 7.57 ± 1.77% and 1.14 ± 0.04 or 1.07 ± 0.02, respectively (Figs. 4G and H). These results indicate that even in the growth medium, overproduction of Six1 promotes differentiation, whereas overproduction of Six4 or Six5 represses differentiation of muscle satellite cells.

Overproduction of Six4 or Six5 inhibits differentiation of satellite cells by down-regulation of myogenin expression

To determine the mechanism of Six1-induced enhancement and Six4-/Six5-induced inhibition of differentiation of satellite cells, we investigated the expression of key regulators of muscle differentiation and regeneration (Fig. 5).

Myogenin is expressed in myoblasts and plays an important role in muscle development [34,35] and its expression is positively controlled by *Six* genes [21,26,27]. The percentage of myogenin-positive cells in EGFP-positive satellite cells infected with the control retrovirus was 18.9 ± 1.68% (Figs. 5A, E, arrows and Q). Overexpression of *Six1* significantly increased the number of myogenin-positive cells to 27.5 ± 3.33% of EGFP-positive cells (Figs. 5B, F, arrows and Q). In contrast, the percentages of myogenin-positive cells were significantly reduced to 4.18 ± 1.71% and 2.49 ± 1.11% in satellite cells infected with the retrovirus harboring *Six4* and *Six5*, respectively (Figs. 5C, D, G, H, arrowheads and Q). These data suggest that misexpression of *Six1* promotes the expression of myogenin, whereas overexpression of *Six4* and *Six5* results in down-regulation of myogenin.

To investigate the effects of overproduction of Six proteins on the activation of muscle satellite cells, we analyzed the expression of MyoD and Pax7. Damage or injury of the skeletal muscle activates quiescent satellite cells as evident by coexpression of MyoD and Pax7 [3]. Following the induction of MyoD and Pax7 expression, most satellite cells undergo proliferation. Infection of satellite cells with the

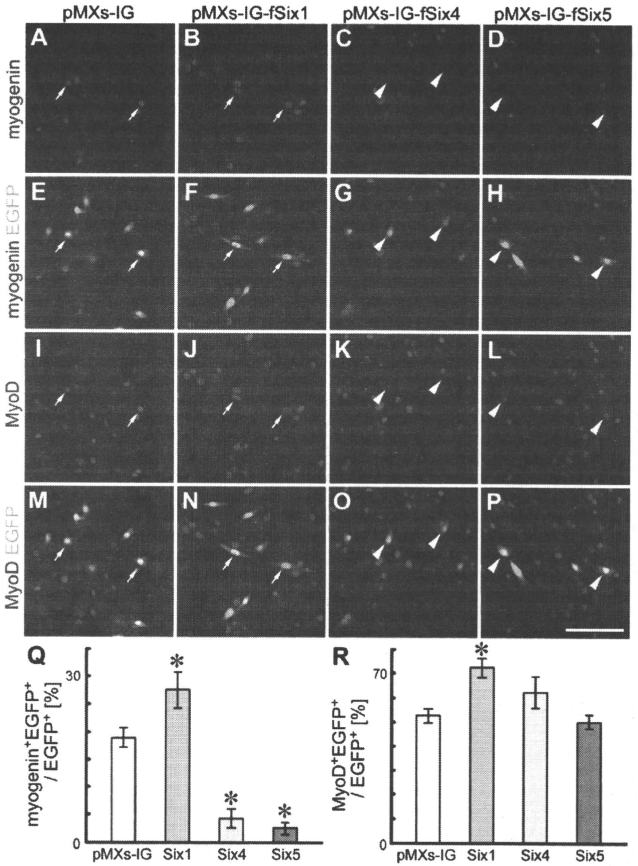

Fig. 5 – Effects of overproduction of Six proteins on the expression of myogenin and MyoD in muscle satellite cells. Immunofluorescence of satellite cells infected with control retrovirus (A, E, I and M) or retrovirus harboring *Six1* (B, F, J and N), *Six4* (C, G, K and O) or *Six5* (D, H, L and P) in growth medium using antibodies to myogenin (A–H in red) and MyoD (I–P in red). Arrows show colocalization of myogenin, MyoD and EGFP. Arrowheads point to weak signals of myogenin immunofluorescence in MyoD and EGFP-positive cells. Scale bar: 100 μm. The percentages of myogenin- and MyoD-positive cells were calculated among the EGFP-positive cells (Q and R). Data are mean ± SEM calculated from three similar results obtained from two independent cell isolates. *$p < 0.05$, compared with pMXs-IG.

control retrovirus resulted in the appearance of MyoD immunofluorescence in the nuclei of 53.9 ± 5.04% of EGFP-positive cells (Figs. 5I, M, arrows and R). The percentages of MyoD-positive cells increased significantly to 72.2 ± 3.95% with retrovirus harboring *Six1* (Figs. 5J, N, arrows and R), but only to 61.8 ± 6.45% and 50.0 ± 2.97% with retroviruses harboring *Six4* and *Six5*, respectively, which were not statistically different from that of the control (Figs. 5K, L, O, P, arrowheads and R). Cultured muscle satellite cells also expressed Pax7 (data not shown). The percentages of Pax7-positive cells were not apparently altered by the infections of retroviruses harboring any of the *Six* genes, compared with the control retrovirus (data not shown). The above results indicate that overexpression of *Six4* and

Six5 results in down-regulation of myogenin, without altering MyoD and Pax7 expression, suggesting that overproduction of Six4 or Six5 negatively regulates the differentiation of satellite cells by repressing the expression of myogenin, while they do not affect the activation of these cells.

Six5 knockdown promotes proliferation of muscle satellite cells

We also examined the functions of *Six* genes using the Stealth small interfering RNA (siRNA)-mediated knockdown approach. The knockdown efficiency of each siRNA against individual *Six* genes, *Six1*, *Six4* and *Six5*, was validated in C2C12 cell line (Supplementary Fig. 2). In muscle satellite cells derived from the extensor digitorum longus (EDL) of 8- to 12-week-old wild-type mice, the endogenous level of Six proteins was not affected by the transfection of negative control siRNA (Fig. 6A, data not shown). The use of Six1 siRNA, Six4 siRNA and Six5 siRNA reduced Six1, Six4 and Six5 protein levels to around 25%, 25% and 40%, respectively, compared to the negative control, when assayed 48 hours after transfection (Fig. 6A).

To investigate the roles of *Six* genes in the proliferation of muscle satellite cells, cell number was counted at 48 hours after transfection of each siRNA and compared to the number of muscle satellite cells transfected with negative control siRNA (Fig. 6B). Six1 siRNA and Six4 siRNA did not significantly change the proportion of such cells (1.33 ± 0.56 and 0.87 ± 0.12-fold, respectively). In contrast, transfection of Six5 siRNA robustly increased the ratio to 5.4 ± 0.71-fold.

To analyze whether knockdown of *Six* genes altered differentiation properties of muscle satellite cells, we performed immunofluorescence of skeletal muscle myosin to assess the extent of muscle differentiation. Twelve hours after transfection of each siRNA, the medium was replaced with the differentiation medium and cells were incubated for additional 36 hours. The proportion of

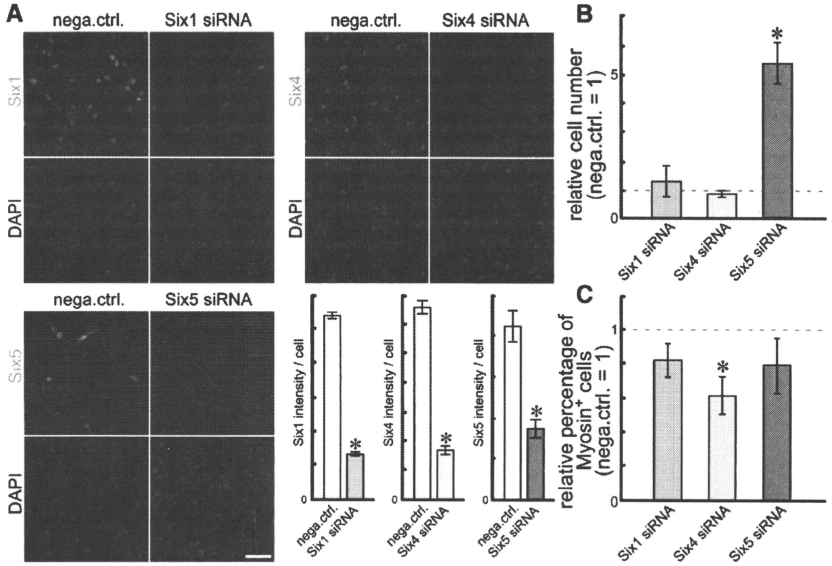

Fig. 6 – Effects of knockdown of *Six1*, *Six4* and *Six5* on proliferation and differentiation of satellite cells. (A) Immunofluorescence of satellite cells transfected with negative control siRNA, Six1 siRNA, Six4 siRNA and Six5 siRNA in growth medium using antibodies to Six1, Six4 and Six5 shown in green. Nuclei were stained with DAPI (blue). The intensity of immunofluorescence of typical result was densitometrically analyzed and displayed in bar graphs. Data are mean ± SEM. *$p < 0.01$, compared with negative control siRNA. Scale bar: 50 μm. Note no obvious increase in picnotic nuclei stained with DAPI in the siRNA-transfected cells, suggesting the marginal cytotoxicity caused by Stealth siRNA. (B) Forty-eight hours after transfection of siRNAs, the cell numbers transfected with Six1 siRNA, Six4 siRNA and Six5 siRNA were counted and normalized by that of negative control siRNA. Data are mean ± SEM of three independent cell isolates. *$p = 0.004$, compared with negative control siRNA. (C) Satellite cells were transfected with siRNAs and cultured in differentiation medium. The percentage of skeletal muscle myosin-positive cells among total cells treated with Six1 siRNA, Six4 siRNA and Six5 siRNA was determined and expressed relative to that of negative control siRNA. Data are mean ± SEM of four independent cell isolates. *$p = 0.01$, compared with the negative control siRNA.

skeletal muscle myosin-positive cells among total cells was determined and normalized by that of muscle satellite cells transfected with negative control siRNA (Fig. 6C). The relative ratios of skeletal muscle myosin-positive cells were reduced to 0.81 ± 0.10, $0.61 \pm 0.11$and 0.79 ± 0.16-fold by the transfection of Six1 siRNA, Six4 siRNA and Six5 siRNA, respectively. However, only the reduction provided by Six4 siRNA was statistically significant. These results indicate that Six5 regulates the proliferation of muscle satellite cells while Six4 plays a role in the differentiation of these cells.

Altered proliferation of muscle satellite cells in $Six4^{+/-}Six5^{-/-}$ mice

We further analyzed the roles of *Six* genes in the proliferation and differentiation of muscle satellite cells by characterizing these cells in *Six* gene-deficient mice. Such analysis would corroborate the data obtained from siRNA-mediated knockdown experiments. However, among the knockout mice of *Six* genes, $Six1^{-/-}$ mice die immediately after birth [11] and it is impossible to analyze satellite cells derived from adult skeletal muscles. Since $Six4^{-/-}$ and $Six5^{-/-}$ mice are viable and do not show apparent muscle phenotypes [16,24,36] (and data not shown), we intercrossed $Six4^{+/-}Six5^{+/-}$ mice to obtain adult with the smallest dosage of *Six* genes. All $Six4^{-/-}Six5^{-/-}$ mice were never born and $Six4^{-/-}Six5^{+/-}$ mice were rarely born in less than Mendelian ratio (data not shown). On the other hand, $Six4^{+/-}Six5^{-/-}$ mice were viable and did not show obvious phenotype in adult skeletal muscles (data not shown). Thus, we were able to evaluate the behavior of satellite cells with the smallest dosage of *Six* genes in $Six4^{+/-}Six5^{-/-}$ mice.

SM/C-2.6-positive cells were isolated from limb and back muscles of 8- to 12-week-old $Six4^{+/-}Six5^{-/-}$ mice and their proliferation and differentiation were compared with those of age-matched wild-type mice (Fig. 7). The total number of muscle satellite cells isolated from $Six4^{+/-}Six5^{-/-}$ mice was not significantly different from those of wild-type mice (data not shown). The isolated satellite cells were plated at two different densities, 6.5×10^3 and 1.3×10^4 cells/cm^2 (Fig. 7A plating) and cultured in the growth medium. The cells were harvested and counted every day for 4 days after plating. One day after plating at low density (6.5×10^3 cells/cm^2), the cell density of satellite cells from $Six4^{+/-}Six5^{-/-}$ mice was significantly higher than that from wild-type mice (Fig. 7A day 1, solid circles). From day 1 to day 4, the density of satellite cells from $Six4^{+/-}Six5^{-/-}$ was consistently higher than that from wild-type (Fig. 7A day 1–day 4, solid circles). When the culture contained a higher density of these cells (1.3×10^4 cells/cm^2), the density of satellite cells from $Six4^{+/-}Six5^{-/-}$ was also consistently higher than that from wild-type after plating (Fig. 7A day 1–day 4, solid squares). Although the satellite cells derived from both genotypes reached a proliferation plateau at 3 days after plating, the cell density at the plateau was also higher in the $Six4^{+/-}Six5^{-/-}$ mice than in wild-type mice (Fig. 7A day 3–day 4, solid squares). Considered together, these results suggest that satellite cells from $Six4^{+/-}Six5^{-/-}$ begin proliferation earlier and grow to a higher cell density, compared to wild-type satellite cells. The possibilities that the observed differences were due to the plating efficiency of the cells or recovery from passage were not excluded.

To analyze whether muscle satellite cells from $Six4^{+/-}Six5^{-/-}$ mice have altered differentiation properties, the satellite cells from wild-type and $Six4^{+/-}Six5^{-/-}$ mice were cultured in the differentiation medium at two different densities, 2×10^4 and 4×10^4 cells/cm^2. We performed immunofluorescence of skeletal muscle myosin to estimate the extent of muscle differentiation. At plating

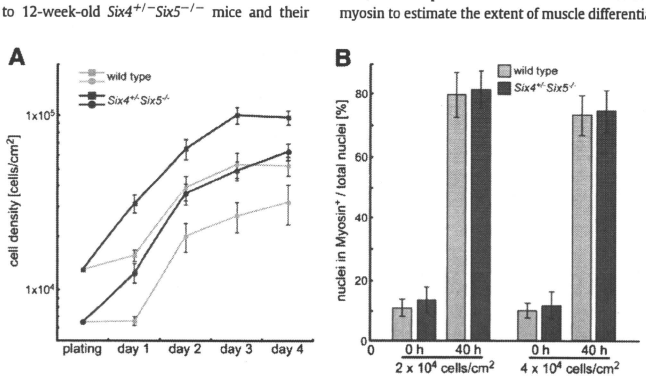

Fig. 7 – Proliferation of muscle satellite cells from $Six4^{+/-}Six5^{-/-}$ and wild-type mice. (A) Isolated satellite cells were plated at two different densities, 6.5×10^3 (circles) and 1.3×10^4 (squares) cells/cm^2. After plating, the cell densities of satellite cells from the wild-type (gray symbols) and $Six4^{+/-}Six5^{-/-}$ (black symbols) mice were calculated at 1 day (day 1), 2 days (day 2), 3 days (day 3) and 4 days (day 4) in the growth medium. Data are mean ± SEM of three independent cell isolates. (B) Satellite cells from wild-type (gray bars) and $Six4^{+/-}Six5^{-/-}$ (black bars) mice were plated at two different densities, 2×10^4 (left side) and 4×10^4 (right side) cells/cm^2. Two hours later, the culture medium was replaced with the differentiation medium to induce differentiation of myotubes. The percentage of nuclei of the satellite cells positive for skeletal muscle myosin immunofluorescence was calculated at medium change to differentiation medium (0 h) and 40 hours after medium change (40 h). Data are mean ± SEM of four independent cell isolates.

(one passage after preparation), the percentage of satellite cells expressing skeletal muscle myosin was not significantly different between wild-type and *Six4*$^{+/-}$*Six5*$^{-/-}$ (data not shown). Two hours after plating, the medium was replaced with the differentiation medium. Satellite cells were collected at 0 and 40 hours after the medium change. At 0 hour, the percentages of skeletal muscle myosin-positive satellite cells were similar in the wild-type (10.7±2.79%) and *Six4*$^{+/-}$*Six5*$^{-/-}$(13.4±4.29%), when plated at low cell density (2×10^4 cells/cm^2) (Fig. 7B 0 h). At 40 hours after the medium change, the percentage of skeletal muscle myosin-positive cells in wild-type (79.5±7.51%) was similar to that in *Six4*$^{+/-}$*Six5*$^{-/-}$ (81.2±6.30%, Fig. 7B 40 h). Even when satellite cells were plated at high density (4×10^4 cells/cm^2), the percentages of skeletal muscle myosin-positive cells in the wild-type were not significantly different from *Six4*$^{+/-}$*Six5*$^{-/-}$ at 0 and 40 hours (9.91±2.57 and 11.7±4.49% at 0 hour, 73.0±6.34 and 74.3±6.73% at 40 hours, respectively). These results suggest that the differentiation capacity of *Six4*$^{+/-}$*Six5*$^{-/-}$ satellite cells is similar to that of the wild-type. Considered together, the analysis of satellite cells from *Six4*$^{+/-}$*Six5*$^{-/-}$ mice indicates that either *Six4* or *Six5* or both play a role in the regulation of muscle satellite cell proliferation.

Discussion

Muscle satellite cells are one of the most important players in muscle regeneration. Understanding the control mechanisms of their proliferation and differentiation is important for the development of cell-based therapy for muscle disorders such as dystrophy using these cells [37]. The roles of the members of *Six* family genes, especially *Six1*, *Six4* and *Six5*, have been extensively studied during embryonic development of skeletal muscle and the results indicate that they play critical roles in myogenesis [21–23]. However, the involvement of these genes in muscle regeneration and behavior of satellite cells has never been addressed. This study demonstrated, for the first time, the roles of *Six* family genes in muscle satellite cells.

Robust induction of Six1- and Six4-positive cells was observed in regenerating muscle three days after damage by cardiotoxin injection in adult skeletal muscle (Fig. 1). Many of these cells were also positive for MyoD, which is known to be expressed in myoblasts produced rapidly during regeneration, and mitotic marker Ki67. Thus, these cells are considered to be myogenic precursor cells. The quiescent muscle satellite cells marked by Pax7 and M-cadherin in the myofibers were also positive for Six1 and Six4 (Fig. 2). In addition, the muscle satellite cells isolated by SM/C-2.6 antibody are positive for Six1, Six4 and Six5 under proliferation and differentiation conditions (Fig. 2). These observations prompted us to investigate in detail the roles of Six1, Six4 and Six5 in the proliferation and differentiation of muscle satellite cells.

One of the intriguing findings of our study is that *Six* genes were involved in the control of cell proliferation of muscle satellite cells. Overexpression of *Six1*, *Six4* or *Six5* in isolated muscle satellite cells inhibited the proliferation as observed by a reduction in the number of cells positive for phospho-histone H3 and Ki67 (Fig. 3). Conversely, siRNA-mediated knockdown of *Six5* resulted in a robust increase in cell number (Fig. 6). These results mean that the proliferation of muscle satellite cells is negatively regulated when the amount of Six proteins exceeds the normal level, while it is normally repressed by Six5 protein present in the cells. These findings highlight the primary repressive role of Six5 in proliferation of activated satellite cells. Moreover, muscle satellite cells from *Six4*$^{+/-}$*Six5*$^{-/-}$ mice proliferated to higher cell density (Fig. 7), consistent with the role of *Six5* defined in overexpression and knockdown experiments. Because we observed the proliferation of isolated satellite cells, the effect of decreased gene dosage of *Six4* and *Six5* is not through altered niche but is rather cell-autonomous change within the satellite cells. Since inactivation of p16^{INK4a}/cyclinD1/Rb pathway is reported to cause rapid and prolonged mitogenic stimulation [38,39], which is reminiscent of the satellite cells from *Six4*$^{+/-}$*Six5*$^{-/-}$ mice, further analysis of the contribution of Six proteins to the regulatory components of cell cycle is required. Reducing the amount of Six5 protein in muscle satellite cells lead to efficient amplification of the cells without changing the differentiation properties (Fig. 6). This remarkable finding suggests that Six5 may be a good candidate as a molecular target in terms of satellite cell therapy. The amount of Six proteins is maintained at critical level for the normal proliferation of satellite cells. Moreover, variable amount and subcellular localization of each of the Six proteins in individual satellite cells might correlate with their function on proliferation and differentiation (Figs. 1 and 2). These aspects of the Six proteins need to be elucidated in the future.

Six1$^{-/-}$ mice show low cell proliferation capacity in the mouse otic vesicle [11,12]. Overexpression of *Xenopus Optix2*, one of the members of *Xenopus Six* family genes, causes retinal field enlargement due to the augmented proliferation [40]. Six proteins influence the cell cycle by regulating the expression of cyclinA1 [41], c-Myc and cyclinD1 [42,43]. These observations implicate a positive regulatory role for Six proteins in cell proliferation. In sharp contrast, Six proteins repress cell proliferation in muscle satellite cells. This may be related to the function of Six1 in stimulating the differentiation of muscle satellite cells or to cell types that provide different context to Six proteins in terms of their functions.

Another interesting finding is the differential role of Six1 and Six4/Six5 in the control of differentiation of muscle satellite cells. Overproduction of Six1 stimulated muscle differentiation estimated by the fusion index and mean number of nuclei in skeletal muscle myosin-positive cells (Fig. 4). In contrast, overexpression of *Six4* and *Six5* inhibited cell differentiation. The main reason for the differential control of cell differentiation might be related to the differential effects of these Six proteins on the expression of myogenin. In cultured cell transfection assays, Six1, Six2, Six4 and Six5 similarly activated the *myogenin* promoter activity in conjunction with Eya coactivator [26,27]. Similarly, *in vivo*, Six1 and Six4 also activated *myogenin* promoter [26]. In isolated muscle satellite cells, overproduction of Six1 activated the expression of myogenin. In sharp contrast, overproduction of Six4 and Six5 greatly reduced the expression of myogenin (Fig. 5). Thus, Six1 might be the primary Six protein that activates *myogenin* promoter in satellite cells. Indeed, Six1 is known to be required for the proper activation of myogenin in limb muscle development [15]. Moreover, the recent finding of Ski pro-oncogene promotion of C2C12 myoblast differentiation through transcriptional activation of *myogenin* in a complex with Six1 and Eya3 is consistent with this notion [44]. The precise molecular basis for the abovementioned differential effects of Six family proteins on the myogenin

expression is unknown. While it is possible that Six4 and Six5 destabilize the myogenin protein, it is more plausible that the differential effect on myogenin expression is at a transcriptional level. Interestingly, we found a profound reduction in Six1 protein level in the satellite cells upon overexpression of Six4 and Six5 (Supplementary Fig. 3). This suggests the indirect repression mechanisms of myogenin by Six4 and Six5. In this context, the recent report that described the binding of Six1 to the regulatory region of *Six1*, *Six4* and *Six5* [45] supports this notion. Because Six1 shares the binding consensus with Six4 and Six5 [46,47], the possible cross-regulations among *Six* genes has been proposed [45]. On the other hand, Six4 and Six5 may be involved in the direct repression of *myogenin* promoter instead of Six1 that activates the promoter. Considering that Six1 and Six4/Six5 had opposite effects on *myogenin* promoter, it should be noted that Six1 and Six4/Six5 each has a distinct molecular structure. The latter two members have a large C-terminal portion in addition to the conserved Six domain and homeodomain [8,48]. This portion may be involved in the differential function of each Six family protein. If this is the case, it is not surprising that Six1 and Six4/Six5 display differential regulatory role in muscle differentiation.

Because *Six* family genes can modulate the proliferation and differentiation of muscle satellite cells, it is tempting to alter the dosage *Six* genes and analyze their effects on muscle regeneration *in vivo*. We are currently addressing the roles of Six family proteins by examining muscle regeneration in *mdx* mice, in which muscle regeneration occurs more frequently in adults. We are crossing *mdx* mice and defective mice harboring lower gene dosage of *Six* or higher dosage of *Six1*. This approach should uncover the physiological roles of *Six* family genes in the regeneration of skeletal muscles.

Materials and methods

Animals

C57BL/6 mice were purchased from Nihon CLEA (Tokyo, Japan). $Six4^{+/-}$ mice were generated as described previously [16]. $Six5^{+/-}$ mice were generously provided by Dr. S. J. Tapscott [24] and crossed with $Six4^{+/-}$ mice to obtain $Six4^{+/-}Six5^{+/-}$ mice. The intercrosses of $Six4^{+/-}Six5^{+/-}$ mice yielded $Six4^{+/-}Six5^{-/-}$ mice. PCR or Southern blotting was performed to verify the genotypes of offspring as described previously [16,24]. Mice were housed in an environmentally controlled room in the Center for Experimental Medicine of Jichi Medical University, under the guidelines for animal experiments. All experimental protocols were approved by the Ethics Review Committee for Animal Experimentation of Jichi Medical University.

Injection of cardiotoxin

To induce muscle regeneration, cardiotoxin (10 μmol/L 5 μl/body weight (g); Sigma, St. Louis, MO) was injected into the TA muscles of 8- to 12-week-old C57BL/6 mice. Three days after injection, TA muscles were harvested and processed for immunofluorescence.

Immunofluorescence

TA muscles were fixed in 4% paraformaldehyde/phosphate-buffered saline (PBS) for 2 hours at 4 °C. Samples were incubated in 30% sucrose/PBS and then embedded in optimal cutting temperature (OCT) compound (Sakura Finetek, Torrance, CA) for freezing and cryosectioning (10–12 μm in thickness). Cultured cells were fixed with 4% paraformaldehyde/PBS for 10 minutes. The following primary antibodies were used in immunofluorescence: guinea pig anti-Six1 antibody (1:5000 dilution [18]), rat anti-Six1 antibody (1:2000 dilution [10]), guinea pig anti-Six4 antibody (1:2000 dilution, [10]), affinity-purified rabbit anti-Six5 antibody (1:500 dilution, [49]), rabbit anti-laminin antibody (1:1500 dilution, Sigma), rabbit anti-MyoD antibody (1:500 dilution, Santa Cruz Biotechnology, Santa Cruz, CA), mouse anti-Pax7 antibody (hybridoma supernatant, Developmental Studies Hybridoma Bank), rabbit anti-M-cadherin antibody (1:1000 dilution, [50]), mouse anti-skeletal muscle myosin antibody (MY-32) (1:30 dilution, Zymed, San Francisco, CA), rabbit anti-phospho-histone H3 (Ser10) antibody (1:1000 dilution, Millipore, Billerica, MA), rabbit anti-Ki67 antibody (1:30 dilution, YLEM, Italy) and mouse anti-myogenin antibody (F5D) (1:500 dilution, Santa Cruz Biotechnology). For anti-Pax7 antibody, M.O.M. Mouse Ig Blocking Reagent (Vector Laboratories, Burlingame, CA) was used to eliminate the background from endogenous mouse immunoglobulins. To visualize the immunoreactions of primary antibodies, fluorescent-labeled secondary antibodies were used at 1:2000 dilution as follows: anti-rabbit conjugated Cy5 (Amersham Biosciences, Piscataway, NJ), Alexa Fluor 488 anti-rabbit, Alexa Fluor 488 anti-rat, Alexa Fluor 488 anti-guinea pig, Alexa Fluor 546 anti-mouse, Alexa Fluor 546 anti-rabbit, Alexa Fluor 546 anti-rat, Alexa Fluor 546 anti-guinea pig and Alexa Fluor 633 anti-mouse (Molecular Probes/Invitrogen, Carlsbad, CA). 4′6-Diamidino-2-phenylindole (DAPI, Sigma) was used at 50 ng/ml to stain nuclei. The immunofluorescent images were captured with Olympus FV1000 confocal microscope and electronically assigned to red, green or blue channels (Olympus Optical, Tokyo, Japan).

Isolation of satellite cells

Muscle satellite cells were isolated from limb and back muscles of 8- to 12-week-old C57BL/6 or $Six4^{+/-}Six5^{-/-}$ mice by using SM/C-2.6 monoclonal antibody as described previously [4,5]. The sorted cells were expanded on Matrigel (BD, Franklin Lakes, NJ)-coated dishes in a growth medium, DMEM, containing 20% fetal bovine serum, human recombinant bFGF (2.5 ng/ml) (Invitrogen), recombinant muse HGF (25 ng/ml) (R&D Systems) and heparin (5 μg/ml) (Sigma). To induce differentiation of the satellite cells, the growth medium was replaced with differentiation medium (2% horse serum/DMEM). The culture medium was replaced with a fresh medium every day. Satellite cells derived from EDL were prepared and cultured as described previously [51] and used for siRNA experiments.

Retrovirus vectors and infection

Flag-tagged mouse *Six1*, *Six4* and *Six5* cDNAs [27,52] were cloned into the multiple cloning site upstream of IRES-EGFP of pMXs-IG vector, which was kindly provided by Dr. T. Kitamura [33]. Retroviral particles were produced by transfection of vector plasmids into PLAT-E packaging cells as described previously [33,53]. Muscle satellite cells were plated at 1.3×10^4 cells/cm^2 in growth medium one passage after the preparation. The next day, the medium was replaced with growth medium containing retroviral particles. Two days after infection, the culture medium

was replaced with growth medium or differentiation medium and the cells were incubated for 24 hours for the assays under proliferating condition or differentiation condition, respectively.

Western blotting

Nuclear and cytoplasmic extracts of proliferating muscle satellite cells isolated from 8-week-old *Six4*$^{-/-}$ mice and C2C12 cells were prepared and analyzed by western blotting using anti-Six5 antibody [49] as described previously [27,54].

Fusion index and statistics

Fusion index was calculated as [(number of nuclei in EGFP-positive myotubes (>2 myonuclei) / total nuclei within EGFP-positive cells) × 100%] [55–57]. Differences from the control experiments were tested statistically by the Student's *t*-test. All values are expressed as mean ± SEM. A probability of less than 5% was considered statistically significant.

RNA interference

The Stealth RNAi siRNA Negative Control Med GC Duplex and Stealth Select siRNAs targeted to mouse *Six1*, *Six4* and *Six5* were purchased from Invitrogen (Carlsbad, CA). Six1 siRNA is a mixture of equimolar amounts of Six1-MSS237917, Six1-MSS237918 and Six1-MSS237919. Six4 siRNA consists of Six4-MSS209042, Six4-MSS209043 and Six4-MSS209044. Six5 siRNA consists of Six5-MSS277077, Six5-MSS277078 and Six5-MSS277079. Sequences for each siRNA species were provided by the company under license. The transfection of Stealth siRNA into satellite cells isolated from EDL was performed using Lipofectamine RNAiMAX (Invitrogen) as described previously [51] with slight modifications.

Supplementary materials related to this article can be found online at doi:10.1016/j.yexcr.2010.08.001.

Acknowledgments

We thank Stephen J. Tapscott for *Six5*$^{-/-}$ mice and reading the manuscript and Toshio Kitamura for pMXs-IG plasmid and PLAT-E cell. We are grateful to So-ichiro Fukada for providing SM/C-2.6 antibody and for the helpful discussion. We also thank Hiroko Ikeda, Yuki Takano, Kanako Mogi, Yuko Suto and Miho Akima for the excellent technical assistance. This work was supported by Research Grant No. 17A-10 for Nervous and Mental Disorders from the Ministry of Health, Labour and Welfare, Intramural Research Grant No. 20B-13 for Neurological and Psychiatric Disorders of NCNP, Support Program for Scientific Research Platform in Private Universities (SPSRP) to JMU and a grant from The Nakatomi Foundation.

REFERENCES

[1] A. Mauro, Satellite cell of skeletal muscle fibers, J. Biophys. Biochem. Cytol. 9 (1961) 493–495.
[2] A. Otto, H. Collins-Hooper, K. Patel, The origin, molecular regulation and therapeutic potential of myogenic stem cell populations, J. Anat. 215 (2009) 477–497.
[3] P.S. Zammit, J.P. Golding, Y. Nagata, V. Hudon, T.A. Partridge, J.R. Beauchamp, Muscle satellite cells adopt divergent fates: a mechanism for self-renewal? J. Cell Biol. 166 (2004) 347–357.
[4] S. Fukada, S. Higuchi, M. Segawa, K. Koda, Y. Yamamoto, K. Tsujikawa, Y. Kohama, A. Uezumi, M. Imamura, Y. Miyagoe-Suzuki, S. Takeda, H. Yamamoto, Purification and cell-surface marker characterization of quiescent satellite cells from murine skeletal muscle by a novel monoclonal antibody, Exp. Cell Res. 296 (2004) 245–255.
[5] S. Fukada, A. Uezumi, M. Ikemoto, S. Masuda, M. Segawa, N. Tanimura, H. Yamamoto, Y. Miyagoe-Suzuki, S. Takeda, Molecular signature of quiescent satellite cells in adult skeletal muscle, Stem Cells 25 (2007) 2448–2459.
[6] M.A. Serikaku, J.E. O'Tousa, sine oculis is a homeobox gene required for Drosophila visual system development, Genetics 138 (1994) 1137–1150.
[7] B.N. Cheyette, P.J. Green, K. Martin, H. Garren, V. Hartenstein, S.L. Zipursky, The Drosophila sine oculis locus encodes a homeodomain-containing protein required for the development of the entire visual system, Neuron 12 (1994) 977–996.
[8] K. Kawakami, S. Sato, H. Ozaki, K. Ikeda, Six family genes—structure and function as transcription factors and their roles in development, Bioessays 22 (2000) 616–626.
[9] H. Kobayashi, K. Kawakami, M. Asashima, R. Nishinakamura, Six1 and Six4 are essential for Gdnf expression in the metanephric mesenchyme and ureteric bud formation, while Six1 deficiency alone causes mesonephric-tubule defects, Mech. Dev. 124 (2007) 290–303.
[10] Y. Konishi, K. Ikeda, Y. Iwakura, K. Kawakami, Six1 and Six4 promote survival of sensory neurons during early trigeminal gangliogenesis, Brain Res. 1116 (2006) 93–102.
[11] H. Ozaki, K. Nakamura, J. Funahashi, K. Ikeda, G. Yamada, H. Tokano, H.O. Okamura, K. Kitamura, S. Muto, H. Kotaki, K. Sudo, R. Horai, Y. Iwakura, K. Kawakami, Six1 controls patterning of the mouse otic vesicle, Development 131 (2004) 551–562.
[12] W. Zheng, L. Huang, Z.B. Wei, D. Silvius, B. Tang, P.X. Xu, The role of Six1 in mammalian auditory system development, Development 130 (2003) 3989–4000.
[13] P.X. Xu, W. Zheng, L. Huang, P. Maire, C. Laclef, D. Silvius, Six1 is required for the early organogenesis of mammalian kidney, Development 130 (2003) 3085–3094.
[14] C. Laclef, E. Souil, J. Demignon, P. Maire, Thymus, kidney and craniofacial abnormalities in Six 1 deficient mice, Mech. Dev. 120 (2003) 669–679.
[15] C. Laclef, G. Hamard, J. Demignon, E. Souil, C. Houbron, P. Maire, Altered myogenesis in Six1-deficient mice, Development 130 (2003) 2239–2252.
[16] H. Ozaki, Y. Watanabe, K. Takahashi, K. Kitamura, A. Tanaka, K. Urase, T. Momoi, K. Sudo, J. Sakagami, M. Asano, Y. Iwakura, K. Kawakami, Six4, a putative myogenin gene regulator, is not essential for mouse embryonal development, Mol. Cell. Biol. 21 (2001) 3343–3350.
[17] G. Oliver, R. Wehr, N.A. Jenkins, N.G. Copeland, B.N. Cheyette, V. Hartenstein, S.L. Zipursky, P. Gruss, Homeobox genes and connective tissue patterning, Development 121 (1995) 693–705.
[18] K. Ikeda, S. Ookawara, S. Sato, Z. Ando, R. Kageyama, K. Kawakami, Six1 is essential for early neurogenesis in the development of olfactory epithelium, Dev. Biol. 311 (2007) 53–68.
[19] Y. Suzuki, K. Ikeda, K. Kawakami, Regulatory role of Six1 in the development of taste papillae, Cell Tissue Res. 339 (2010) 513–525.
[20] K. Ikeda, R. Kageyama, Y. Suzuki, K. Kawakami, Six1 is indispensable for production of functional apical and basal progenitors during olfactory epithelial development, Int. J. Dev. Biol. (in press), doi:10.1387/ijdb.093041ki.
[21] R. Grifone, J. Demignon, C. Houbron, E. Souil, C. Niro, M.J. Seller, G. Hamard, P. Maire, Six1 and Six4 homeoproteins are required for Pax3 and Mrf expression during myogenesis in the mouse embryo, Development 132 (2005) 2235–2249.